This is the author's final accepted version.

There may be differences between this version and the published version.
You are advised to consult the publisher's version if you wish to cite from
it.

http://eprints.gla.ac.uk/157932/

Deposited on: 27 February 2018

Redox-Active Metallodithiolene Groups Separated by Insulating Tetraphosphinobenzene Spacers

Kuppuswamy Arumugam,[†] Malathy Selvachandran,[‡] Antony Obanda,[‡] Mohamed C. Shaw,[‡] Perumalreddy Chandrasekaran,[£] Sonya L. Caston Good,[¢] Joel T. Mague,[‡] Stephen Sproules*,[§] and James P. Donahue*,[‡]

Abstract. Compounds of the type $[(S_2C_2R_2)M(\mu\text{-tpbz})M(S_2C_2R_2)]$ (R = CN, Me, Ph, *p*-anisyl; M= Ni, Pd, or Pt; tpbz = 1,2,4,5-tetrakis(diphenylphosphino)benzene) have been prepared by transmetallation with $[(S_2C_2R_2)SnR'_2]$ reagents, by direct displacement of dithiolene ligand from $[M(S_2C_2R_2)_2]$ with 0.5 eq of tpbz, or by salt metathesis using $Na_2[S_2C_2(CN)_2]$ in conjunction with $X_2M(\mu\text{-tpbz})MX_2$ (X = halide). X-ray crystallography reveals a range of topologies (undulating, chair, bowed) for the $(S_2C_2)M(P_2C_6P_2)M(S_2C_2)$ core. The $[(S_2C_2R_2)M(\mu\text{-tpbz})M(S_2C_2R_2)]$ (R = Me, Ph, *p*-anisyl) compounds support reversible or quasi-reversible oxidations corresponding to concurrent oxidation of the dithiolene terminal ligands from ene-1,2-dithiolates to radical monoanions, forming $[((^-S^\bullet SC_2R_2)M(\mu\text{-tpbz})M(^-S^\bullet SC_2R_2)]^{2+}$. The R = Ph and *p*-anisyl compounds support a second, reversible oxidation of the dithiolene ligands to their α-dithione form. In contrast, $[(S_2C_2(CN)_2)Ni(tpbz)Ni(S_2C_2(CN)_2)]$ sustains only reversible, metal-centered reductions. Spectroscopic examination of $[(^-S^\bullet SC_2(p\text{-anisyl})_2)_2Ni(\mu\text{-tpbz})Ni(^-S^\bullet SC_2(p\text{-anisyl})_2)_2]^{2+}$ by EPR reveals a near degenerate singlet-triplet ground state, with spectral simulation revealing a remarkably small dipolar coupling constant of 18×10^{-4} cm^{-1} that is representative of an interspin distance of 11.3 Å. This weak interaction is mediated by the rigid tpbz ligand, whose capacity to electronically insulate is an essential quality in the development of molecular-based spintronic devices.

[†]Dept. of Chemistry, Wright State University, 3640 Colonel Glenn Hwy, Dayton, OH 45435-0001, United States
[‡]Dept. of Chemistry, Tulane University, 6400 Freret St., New Orleans, LA 70118-5698, United States
[£]Dept. of Chemistry and Biochemistry, Lamar University, Beaumont, TX 77710, United States
[¢]Dept. of Chemistry, Texas Southern University, 1300 Cleburne Street, Houston, TX 77004, United States
[§]WestCHEM, School of Chemistry, University of Glasgow, Glasgow, G12 8QQ, United Kingdom.

Abstract. Compounds of the type $[(S_2C_2R_2)M(\mu\text{-tpbz})M(S_2C_2R_2)]$ (R = CN, Me, Ph, *p*-anisyl; M= Ni, Pd, or Pt; tpbz = 1,2,4,5-tetrakis(diphenylphosphino)benzene) have been prepared by transmetallation with $[(S_2C_2R_2)SnR'_2]$ reagents, by direct displacement of dithiolene ligand from $[M(S_2C_2R_2)_2]$ with 0.5 eq of tpbz, or by salt metathesis using $Na_2[S_2C_2(CN)_2]$ in conjunction with $X_2M(\mu\text{-tpbz})MX_2$ (X = halide). X-ray crystallography reveals a range of topologies (undulating, chair, bowed) for the $(S_2C_2)M(P_2C_6P_2)M(S_2C_2)$ core. The $[(S_2C_2R_2)M(\mu\text{-tpbz})M(S_2C_2R_2)]$ (R = Me, Ph, *p*-anisyl) compounds support reversible or quasi-reversible oxidations corresponding to concurrent oxidation of the dithiolene terminal ligands from ene-1,2-dithiolates to radical monoanions, forming $[((^-S^{\bullet}SC_2R_2)M(\mu\text{-tpbz})M(^-S^{\bullet}SC_2R_2)]^{2+}$. The R = Ph and *p*-anisyl compounds support a second, reversible oxidation of the dithiolene ligands to their α-dithione form. In contrast, $[(S_2C_2(CN)_2)Ni(tpbz)Ni(S_2C_2(CN)_2)]$ sustains only reversible, metal-centered reductions. Spectroscopic examination of $[(^-S^{\bullet}SC_2(p\text{-anisyl})_2)Ni(\mu\text{-tpbz})Ni(^-S^{\bullet}SC_2(p\text{-anisyl})_2)]^{2+}$ by EPR reveals a near degenerate singlet-triplet ground state, with spectral simulation revealing a remarkably small dipolar coupling constant of 18×10^{-4} cm^{-1} that is representative of an interspin distance of 11.3 Å. This weak interaction is mediated by the rigid tpbz ligand, whose capacity to electronically insulate is an essential quality in the development of molecular-based spintronic devices.
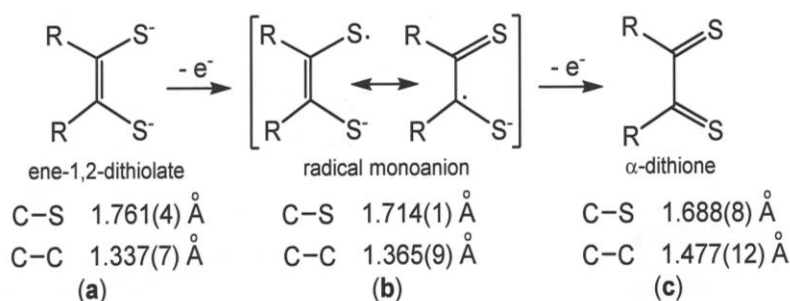
Scheme 1. Redox states of a dithiolene ligand, with approximate intraligand C–S and C–C bond lengths indicated. Bond lengths are taken from the structures of $[Ni(S_2C_2Me_2)_2]^n$ (n = 0, 2– for (a) and (b), respectively,[1] and $[Ni(Me_2pipdt)_2]^{2+}$ (Me₂pipdt = 1,4-dimethylpiperazine-2,3-dithione).[2]

Introduction

One of the defining characteristics of metallodithiolene complexes, both homoleptic and heteroleptic, is highly reversible redox chemistry that is associated with the dithiolene ligand(s). Scheme 1 illustrates the several redox levels that can, in principle, be accessed by a dithiolene ligand along with the intra-ligand bond lengths that are diagnostic of the redox state.[1,2] Rather different behavior can be manifested by the same dithiolene complex in one redox state as compared to another, which creates possibilities for applications that exploit these property differences in an "on-off" way. Examples of these property changes are switching of coordination geometry as function of redox state[3] and binding of an exogenous ligand in one redox state but release of it in another.[4-7] Breakthrough developments in the application of such compounds for smart or advanced materials will likely hinge upon an ability to execute the efficient synthesis of multi-component metallodithiolene compounds in a modular or stepwise
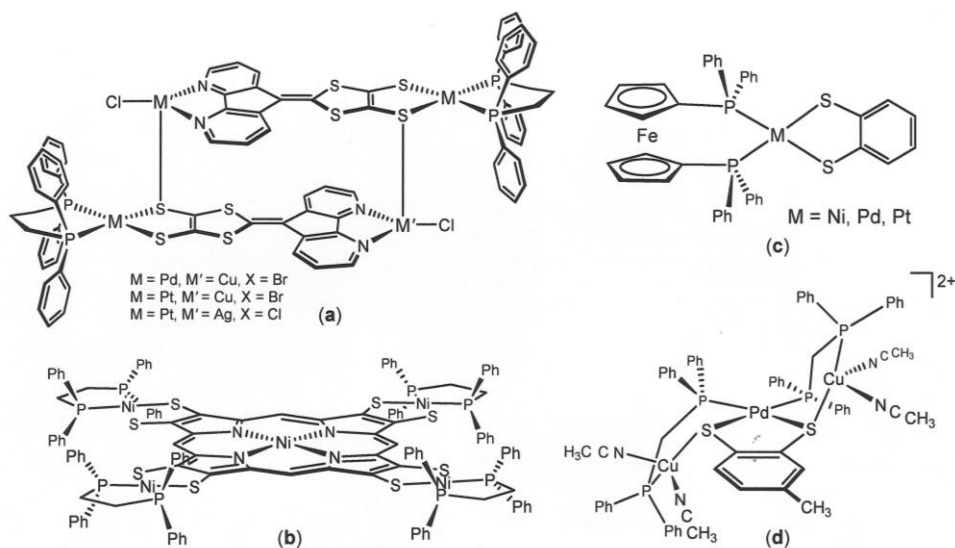

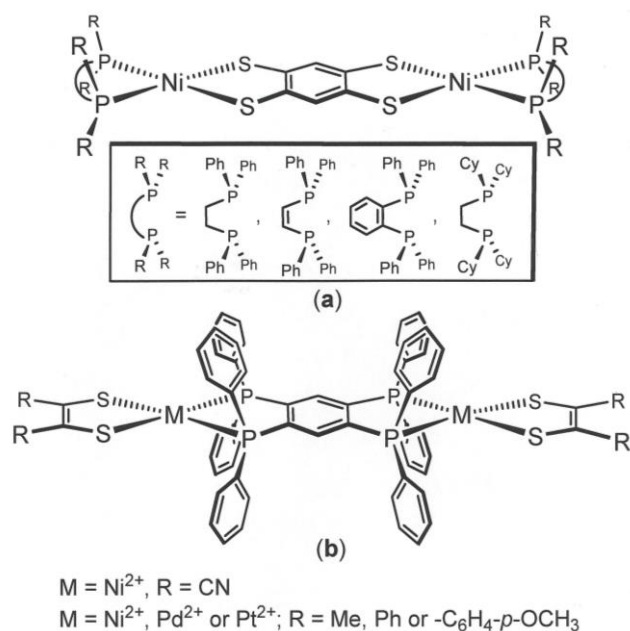**Figure 1**. Representative examples of multi-metal dithiolene complexes.

Figure 2. (a) Dimetallic 1,2,4,5-tetrathiolatobenzene-linked compounds with diphosphine end groups; (b) Dimetallic 1,2,4,5-tetrakis(diphenylphosphino)benzene-linked compounds with dithiolene end groups.

way with precise control of the spatial disposition or separation between such components.

Figure 1 illustrates a representative variety of multi-metal complexes in which both dithiolene ligands and other "functional elements" are incorporated.[8-12] The other functional elements may be structural only, other redox-active centers, chromophores separate from or conjugated to the metallodithiolene moiety, or some combination of the foregoing. In an earlier report[13,14] intended as a prelude to a well-defined set of metallodithiolene oligomers, we described the synthesis and properties of di- and trimetallic 1,2,4,5-tetrathiolatobenzene-linked complexes of the group 10 metals which employed chelating diphosphines as stable, capping end-groups (Figure 2a). The dimetallic compounds displayed two well-separated reversible oxidation waves attributed to oxidation of the 1,2,4,5-tetrathiolatobenzene core to a 2,5-dithiolato thioquinone. The oxidized forms of the compounds displayed a sensitivity that made isolation only possible with a noncoordinating tetraarylborate anion. The ready availability of several types of 1,2,4,5-tetraphosphinobenzene ligands posed the idea of inverting, for effect, the tetrathiobenzene bridge and capping diphosphine for tetraphosphinobenzene bridge and terminal dithiolene ligand (Figure 2b). As described in an initial report,[15] such compounds are redox-active but with near concurrent oxidations of the dithiolene end groups. In this work, we follow upon that initial report with a detailed synthesis, structural, and electrochemical report of an

extensive set of dimetallic compounds in which the group 10 metal ion and dithiolene ligand substituent are varied within a constant 1,2,4,5-tetrakis(diphenylphosphino)benzene core. Selected mono-metallic compounds have also been prepared and studied to assist interpretation of spectral and electrochemical data. The suite of compounds listed in Chart 1 and illustrated in Scheme 2 is the subject of this report, which provides an in-depth study of their structural, electrochemical and spectroscopic properties and clarifies the degree of tunability they offer for the design of weakly-coupled, reversibly accessible unpaired spins.

Chart 1. Numbering for Compound Identification

[(mnt)Ni(dppb)]	**1**
[(mdt)Ni(dppb)]	**2**
[(mdt)Pd(dppb)]	**3**
[(adt)Ni(dppb)]	**4**
[(adt)Pd(dppb)]	**5**
[(adt)Pt(dppb)]	**6**
[Cl$_2$Ni(μ-tpbz)NiCl$_2$]	**7**
[Br$_2$Ni(μ-tpbz)NiBr$_2$]	**8**
[Cl$_2$Pd(μ-tpbz)PdCl$_2$]	**9**
[(mnt)Ni(μ-tpbz)Ni(mnt)]	**10**
[(mdt)Ni(μ-tpbz)Ni(mdt)]	**11**
[(mdt)Pd(μ-tpbz)Pd(mdt)]	**12**
[(mdt)Pt(μ-tpbz)Pt(mdt)]	**13**
[(pdt)Ni(μ-tpbz)Ni(pdt)]	**14**
[(pdt)Pd(μ-tpbz)Pd(pdt)]	**15**
[(pdt)Pt(μ-tpbz)Pt(pdt)]	**16**
[(adt)Ni(μ-tpbz)Ni(adt)]	**17**
[(adt)Pd(μ-tpbz)Pd(adt)]	**18**
[(adt)Pt(μ-tpbz)Pt(adt)]	**19**

Experimental

General Considerations. Literature procedures were employed for the syntheses of 1,2-bis(diphenylphosphino)benzene (dppb),[16] 1,2,4,5-tetrakis(diphenylphosphino)benzene (tpbz),[17] disodium 1,2-dicyano-ene-1,2-dithiolate (Na$_2$(S$_2$C$_2$(CN)$_2$), Na$_2$mnt),[18] 4,5-dimethyl-1,3-dithiol-2-one,[19] 4,5-bis(4-methoxyphenyl)-1,3-dithiol-2-one,[20] 2,2-dimethyl-4,5-dicyano-1,3,2-dithiastannole ([(mnt)SnMe$_2$]),[21] 2,2-dimethyl-4,5-bis(4-methoxyphenyl)-1,3,2-dithiastannole,[20] 2,2-di-n-butyl-4,5-dimethyl-1,3,2-dithiastannole ([(mdt)Sn^{n}Bu$_2$]),[22] [Cl$_2$M(dppb)] (M = Ni,[23] Pd[24]), [NiCl$_2$(dme)][25] (dme = 1,2-dimethoxyethane), [Cl$_2$Pt(μ-tpbz)PtCl$_2$],[26] [M(pdt)$_2$][27] (pdt =

5

1,2-diphenyl-1,2-ethylenedithiolate; M = Ni, Pd, Pt), [PdCl$_2$(cod)] (cod = 1,5-cyclooctadiene),[28] [(adt)Pd(dppb)],[15] and [(adt)Pd(μ-tpbz)Pd(adt)], **18** (adt = 1,2-di-*p*-anisyl-1,2-ethylenedithiolate).[15] All other reagents were purchased from commercial sources and used as received. Solvents either were dried with a system of drying columns from the Glass Contour Company (CH$_2$Cl$_2$, *n*-pentane, hexanes, Et$_2$O, THF, C$_6$H$_6$, toluene) or freshly distilled according to standard procedures (MeOH, CH$_3$CN, 1,2-dichloroethane).[29] All reactions described below were conducted under an atmosphere of N$_2$, while silica columns were run in the open air using 60-230 micron silica (Dynamic Adsorbents).

Syntheses.

[(mnt)Ni(dppb)], **1**. The following procedure is a modification of a published preparation.[9] A mixture of [NiCl$_2$(dppb)] (0.100 g, 0.17 mmol) and [(mnt)SnMe$_2$] (0.75 g, 2.6 mmol) was dissolved in dichloroethane (30 mL) and refluxed with stirring for 2 h. The resulting reddish-brown colored solution was then cooled to ambient temperature, and the solvent was removed under reduced pressure. The residual solid was washed with MeOH (2 × 3 mL) followed by Et$_2$O (2 × 5 mL) and then dried under vacuum. Yield: 0.091 g, 81%. ^{31}P NMR (δ, ppm in CD$_2$Cl$_2$): 58.9 (s). UV-vis (CH$_2$Cl$_2$), λ$_{max}$ (ε, 10^4 M^{-1} cm^{-1}): ~435 (sh, ~0.12), 550 (0.02). MS (MALDI-TOF) *m/z*: 666.5 (M + Na$^+$).

[(mdt)Ni(dppb)], **2**. A 50 mL Schlenk flask was charged with [(mdt)Sn^{n}Bu$_2$] (0.100 g, 0.285 mmol) and [Cl$_2$Ni(dppb)] (0.164 g, 0.285 mmol). To this mixture of solids was added 25 mL CH$_2$Cl$_2$, which occasioned an immediate change in color from orange to green. This solution was stirred overnight at ambient temperature and then was evaporated to dryness under reduced pressure. The residual solid was washed with MeOH (3 × 10 mL) and Et$_2$O (3 × 10 mL) and dried again *in vacuo* to afford a green solid. Yield: 0.160 g, 90%. Recrystallization was readily accomplished by the diffusion of *n*-pentane vapor into a filtered CH$_2$Cl$_2$ solution. R$_f$ (CH$_2$Cl$_2$): 0.58. ^{1}H NMR (CD$_2$Cl$_2$): δ 7.70-7.33 (multiple overlapped signals, 24H, aromatic C-*H*), 2.00 (s, 6H, -C*H$_3$*). ^{31}P NMR (δ, ppm in CD$_2$Cl$_2$): 56.16 (s). UV-vis (CH$_2$Cl$_2$), λ$_{max}$ (ε, 10^4 M^{-1} cm^{-1}): 404 (0.23), 626 (0.02). MS (MALDI-TOF) *m/z*: 622.8 (M$^+$).

[(mdt)Pd(dppb)], **3**. A 50 mL Schlenk flask was charged with [Cl$_2$Pd(dppb)] (0.050 g, 0.08 mmol) and 25 mL CH$_2$Cl$_2$. To this mixture [(mdt)SnMe$_2$] (0.021 g, 0.08 mmol) was added, and an immediate color change from pale orange to brown was observed. This solution was stirred

overnight at room temperature and then was evaporated to dryness under reduced pressure. The solid product was washed with 5 mL MeOH and 5 mL EtOH and dried under vacuum to afford a brown solid. Yield: 0.034 g, 63%. Recrystallization was accomplished by the diffusion of Et_2O vapor into a filtered CH_2Cl_2 solution. R_f (CH_2Cl_2): 0.46. ^{1}H NMR (δ, ppm in CD_2Cl_2): 7.70-7.33 (multiple overlapped signals, 24H, aromatic C-*H*), 2.00 (s, 6H, -C*H*₃). ^{31}P NMR (δ, ppm in CD_2Cl_2): 56.16 (s). UV-vis (CH_2Cl_2), λ_{max} (ϵ, 10^4 M^{-1} cm^{-1}): 545 (0.01), 403 (0.08), 369 (0.09).

[(adt)Ni(dppb)], **4**. A procedure analogous to that employed for the synthesis and purification of **2** was used but with [(adt)SnMe₂] (0.100 g, 0.222 mmol) used in place of [(mdt)Sn^{n}Bu₂]. Yield: 0.120 g, 67%. ^{1}H NMR (δ, ppm in CD_2Cl_2): 7.58 (m, 8H, aromatic C-*H*), 7.48 (m, 2H, aromatic C-*H*), 7.38-7.35 (m, 6H, aromatic C-*H*), 7.30-7.27 (m, 8H, aromatic C-*H*), 6.97 (d, J = 8.4 Hz, 4H, aromatic C-*H*), 6.52 (d, J = 8.4 Hz, 4H, aromatic C-*H*), 3.60 (s, 6H, -OC*H*₃) ^{31}P NMR (δ, ppm in CD_2Cl_2): 56.31 (s). UV-vis (CH_2Cl_2), λ_{max} (ϵ, 10^4 M^{-1} cm^{-1}): ~406 (sh, ~0.42), 618 (0.07). MS (MALDI-TOF) m/z: 807.1 (M[+]). HRMS (MALDI-TOF): monoisotopic m/z: 806.1154 (calcd for $C_{46}H_{38}NiO_2P_2S_2$ (M[+]) 806.1135). Anal. Calcd for $C_{46}H_{38}NiO_2P_2S_2$: C, 68.42; H, 4.74; P, 7.67. Found: C, 68.25; H, 4.73; P, 7.75.

[(adt)Pt(dppb)], **6**. A mixture of [Pt(adt)₂] (0.030 g, 0.038 mmol) and dppb (0.017 g, 0.037 mmol) in 1,2-dichloroethane (30 mL) was stirred and refluxed for 12 h, during which time the solution developed a brown color. After the mixture cooled to ambient temperature, the solvent was evaporated under reduced pressure. The residual solid was redissolved in CH_2Cl_2, evaporated onto dry silica (~1 g), and dry-loaded onto a silica column packed as a slurry in 1:1 CH_2Cl_2/hexanes. Elution with this same solvent mixture brought a brown band of unreacted [Pt(adt)₂] down the column. Following collection of this leading band, continued elution with pure CH_2Cl_2 moved a yellowish band of [(adt)Pt(dppb)], which was collected and reduced to dryness to afford **6**. Yield: 0.026 g (76%). R_f (CH_2Cl_2): 0.76. ^{1}H NMR (δ, ppm in CD_2Cl_2): δ 7.71 (m, 8H, aromatic C-*H*), 7.64 (m, 2H, aromatic C-*H*), 7.58 (m, 2H, aromatic C-*H*), 7.49-7.39 (m, 12 H, aromatic C-H) 7.06 (d, 4H, aromatic C-*H* of adt ligand), 6.62 (d, 4H, aromatic C-*H* of adt ligand), 3.70 (s, 6H, -OC*H*₃). ^{31}P NMR (δ, ppm in CD_2Cl_2): 44.67 (s). UV-vis (CH_2Cl_2), λ_{max} (ϵ, 10^4 M^{-1} cm^{-1}): ~330 (sh, 0.50), 390 (0.21). MS (MALDI-TOF) m/z: 943.1 (M[+]).

[Cl₂Ni(μ-tpbz)NiCl₂], **7**. A 25 mL Schlenk flask was charged with [NiCl₂(dme)] (0.054 g, 0.245 mmol), tpbz (0.100 g, 0.123 mmol) and 1,2-dichloroethane (15 mL), and the mixture was stirred under reflux for 12 h. A color change from pale yellow to orange was noted. After cooling

7

to ambient temperature, the yellow precipitate in the flask was collected by filtration in the open air, washed with EtOH (3 × 10 mL) followed by Et_2O (3 × 10 mL), and dried under vacuum. Yield: 0.093 g, 71%. UV-vis ($C_6H_5NO_2$), λ_{max} nm (ε, 10^4 M^{-1} cm^{-1}): 460 (0.25).

[Br₂Ni(μ-tpbz)NiBr₂], **8**. A solution of the tpbz ligand (0.100 g, 0.123 mmol) in hot EtOH (15 mL) was added to $NiBr_2 \cdot xH_2O$ (0.054 g) in EtOH (1 mL). A color change from pale red to dark red was observed. The reaction mixture was refluxed overnight while being stirred under a N_2 atmosphere. Upon cooling, the red solid precipitate was recovered by filtration, washed with EtOH (3 × 10 mL) and Et_2O (3 × 10 mL), and dried under vacuum. Yield: 0.105 g, 68% based on tpbz ligand. UV-vis ($C_6H_5NO_2$), λ_{max} nm (ε, 10^4 M^{-1} cm^{-1}): 476 (0.37). Recrystallization of **8** from nitrobenzene produces crystals with two interstitial $C_6H_5NO_2$ molecules per molecule of **8**. Anal Calcd for [Br₂Ni(μ-tpbz)NiBr₂]·$2C_6H_5NO_2$: C, 52.92; H, 3.49; N, 1.87. Found: C, 52.90; H, 3.64; N, 2.41.

[Cl₂Pd(μ-tpbz)PdCl₂], **9**. The following procedure is a modification of a published preparation.[26] A solution of tpbz (0.173 g, 0.212 mmol) in MeCN (15 mL) was treated with a solution of [PdCl₂(cod)] (0.121 g, 0.424 mmol) in CH_2Cl_2 (15 mL) added dropwise via cannula at ambient temperature. The resulting mixture was stirred overnight, and all volatiles were then removed under reduced pressure. The residual solid was washed with Et_2O (2 × 10 mL) and dried under vacuum to afford [Cl₂Pd(μ-tpbz)PdCl₂] an off-white solid. Yield: 0.193 g, 87%. Compound **9** is soluble in DMSO and readily crystallizes from this solvent upon slow introduction of various solvents (C_6H_6, ^tBuOMe, THF, $^iPr_2O$) by vapor diffusion techniques. ^{31}P NMR (δ, ppm in DMSO-d_6): 62.46.

[(mnt)Ni(μ-tpbz)Ni(mnt)], **10**. A 50 mL Schlenk flask was charged with [(mnt)SnMe₂] (0.058 g, 0.20 mmol) and [Br₂Ni(μ-tpbz)NiBr₂] (0.125 g, 0.10 mmol) under a N_2 atmosphere. To this mixture of solids was added 25 mL 1,2-dichloroethane via syringe, and the resulting solution was stirred at 50 °C for 24 h. The solvent was removed under reduced pressure, and the solid residue was triturated in MeOH (15 mL). The solid product was separated from this heterogeneous mixture by filtration in the open air and was washed with additional small portions of MeOH (3 × 5 mL) followed by diethyl ether (3 × 5 mL). Yield: 0.097 g, 80%. MS (MALDI-TOF) m/z: 1211.7369 (M^+). IR (KBr, cm^{-1}): ν(CN) 2215 (m), ν(CN) 2199 (s), 1637 (m), 1501 (m), 1435 (s), 1096 (s), 681 (m), 639 (m).

[(mdt)Ni(μ-tpbz)Ni(mdt)], **11**. A 25 mL Schlenk flask with stir bar was charged with [Cl$_2$Ni(μ-tpbz)NiCl$_2$] (0.153 g, 0.14 mmol), [(mdt)Sn^{n}Bu$_2$] (0.100 g, 0.284 mmol), and dry CH$_2$Cl$_2$ (15 mL). The resulting mixture was stirred for 12 h at 25 °C under N$_2$, during which time the insoluble [Cl$_2$Ni(μ-tpbz)NiCl$_2$] completely dissolved and a homogeneous dark brown solution resulted. This solution was reduced to dryness under vacuum, and the resulting brown residue was washed with MeOH (3 × 5 mL) followed by Et$_2$O (3 × 5 mL). Yield: 0.106 g, 71%. ^{1}H NMR (δ, ppm in CD$_2$Cl$_2$): 7.44-7.40 (m, 24H, aromatic C-H), 7.35-7.31 (m, 2H, P$_2$C$_6$$H_2P_2$ aromatic C-H), 7.29-7.25 (m, 16H, aromatic C-H), 1.97 (s, 12H, dithiolene –CH_3). ^{13}C NMR (δ, ppm in CD$_2$Cl$_2$): 147.8, 136.8, 133.6, 132.2, 131.3, 129.8, 128.7, 20.9. ^{31}P NMR (δ, ppm in CD$_2$Cl$_2$): 55.0. UV-vis (CH$_2$Cl$_2$), λ$_{max}$ (ε, 10^4 M^{-1} cm^{-1}): 308 (sh, 2.49), 478 (0.23). MS (MALDI-TOF) m/z: 1168.4 (M$^+$). Anal. Calcd for C$_{62}$H$_{54}$P$_4$Pd$_2$S$_4$: C, 63.72; H, 4.66; P, 10.60. Found: C, 63.50; H, 4.72; P, 10.36.

[(mdt)Pd(μ-tpbz)Pd(mdt)], **12**. The same procedure and scale described for the synthesis of **11** were employed but with [Cl$_2$Pd(μ-tpbz)PdCl$_2$] used in place of the corresponding dinickel compound. Yield, 0.120 g, 72%. ^{1}H NMR (δ, ppm in CD$_2$Cl$_2$): 7.55-7.51 (m, 2H, P$_2$C$_6$$H_2P_2$ aromatic C-H), 7.47-7.38 (m, 24H aromatic C-H), 7.32-7.29 (m, 16H, aromatic C-H), 1.97 (s, 12H, dithiolene –CH_3). ^{31}P NMR (δ, ppm in CD$_2$Cl$_2$): 46.87. UV-vis (CH$_2$Cl$_2$), λ$_{max}$ (ε, 10^4 M^{-1} cm^{-1}): 268 (sh, 7.24), 484 (0.23). MS (MALDI-TOF) m/z: 1264 (M$^+$). Anal. Calcd for C$_{62}$H$_{54}$P$_4$Pd$_2$S$_4$: C, 58.91; H, 4.31; P, 9.80. Found: C, 59.10; H, 4.36; P, 9.68.

[(mdt)Pt(μ-tpbz)Pt(mdt)], **13**. The same procedure and scale described for the synthesis of **11** were employed but with [Cl$_2$Pt(μ-tpbz)PtCl$_2$] used in place of the corresponding dinickel compound. Yield, 0.163 g, 80%. ^{1}H NMR (δ, ppm in CD$_2$Cl$_2$): 7.63 (br s, 2H, aromatic C-H), 7.47-7.43 (m, 24 H, aromatic C-H), 7.33-7.30 (m, 16H, aromatic C-H), 2.05 (s, 12H dithiolene –CH_3). ^{13}C NMR (δ, ppm in CD$_2$Cl$_2$): 146.9, 137.8, 133.7, 131.7, 130.1, 128.8, 127.5, 22.2. ^{31}P NMR (δ, ppm in CD$_2$Cl$_2$): 41.8 (s, J_{Pt-P} = 2737 Hz). UV-vis (CH$_2$Cl$_2$), λ$_{max}$ (ε, 10^4 M^{-1} cm^{-1}): 350 (sh, 0.49), 472 (0.35). MS (MALDI-TOF) m/z: 1440.7 (M$^+$). Anal. Calcd for C$_{62}$H$_{54}$P$_4$Pt$_2$S$_4$: C, 51.66; H, 3.78; P, 8.60. Found: C, 51.17; H, 3.89; P, 8.65.

[(pdt)Ni(μ-tpbz)Ni(pdt)], **14**. A 25 mL Schlenk flask with stir bar was charged with tpbz (0.100 g, 0.123 mmol) and 20 mL of CH$_2$Cl$_2$. To this stirring mixture was then added [Ni(pdt)$_2$] (0.133 g, 0.245 mmol) under outward N$_2$ flow, and formation of a dark brown color was observed soon thereafter. Stirring was continued overnight, after which time the solvent was

removed under reduced pressure. The residual solid was purified on a silica column packed as a slurry in 2:1 CH_2Cl_2/THF. Elution with this same solvent mixture induced movement of brown band of [(pdt)Ni(μ-tpbz)Ni(pdt)], which was collected and taken to dryness Yield: 0.155 g, 89%. R_f: 0.96 in 2:1 CH_2Cl_2/THF. ^{1}H NMR (δ, ppm in CD_2Cl_2): 7.48 (multiple overlapped signals, ~26H, aromatic C-*H*), 7.33 (t, ~16H, aromatic C-*H*), 7.10 (m, ~8H, aromatic C-*H*), 7.04 (m, ~12H, aromatic C-*H*). ^{31}P NMR (δ, ppm in CD_2Cl_2): 54.31. UV-vis (CH_2Cl_2), λ_{max} nm (ϵ, 10^4 M^{-1} cm^{-1}): 376, (sh, ~0.65), 474 (0.27), 618 (0.05). MS (MALDI-TOF) *m/z*: 1416.3 (M^+).

[(pdt)Pd(μ-tpbz)Pd(pdt)], **15**. A 25 mL Schlenk flask with stir bar was charged with tpbz (0.050 g, 0.061 mmol), [Pd(pdt)$_2$] (0.072 g, 0.122 mmol) and 20 mL CH_2Cl_2. The resulting mixture was stirred overnight, during which time the formation of a maroon color solution was observed. The solvent was removed under vacuum, and the residual solid was redissolved and evaporated onto silica (~0.30 g). The dry-loaded silica was added to the top of a column packed as a slurry in hexanes. Elution with 10:1 CH_2Cl_2/THF moved **15** as a well-resolved maroon-colored band. Yield: 0.069 g, 74%. R_f = 0.85 in 10:1 CH_2Cl_2/THF. ^{31}P NMR (δ, ppm in CD_2Cl_2): 47.9. UV-vis (CH_2Cl_2) λ_{max} nm (ϵ, 10^4 M^{-1} cm^{-1}): 480 (0.09). MS (MALDI-TOF) *m/z*: 1512.3 (M^+).

[(pdt)Pt(μ-tpbz)Pt(pdt)], **16**. The same procedure and scale as described above for **15** were implemented but with [Pt(pdt)$_2$] used in place of [Pd(pdt)$_2$]. However, the silica column used in purifying the crude product was first eluted with 1:1 CH_2Cl_2/hexanes to separate a modest amount of unreacted [Pt(pdt)$_2$]. Continued elution with 10:1 CH_2Cl_2/THF moved **16** as a well-resolved red fraction that was collected separately and reduced to dryness. Yield: 0.062 g, 60%. R_f = 0.94 in 10:1 CH_2Cl_2/THF. ^{31}P NMR (δ, ppm in CD_2Cl_2): 42.3. UV-vis (CH_2Cl_2), λ_{max} nm (ϵ, 10^4 M^{-1} cm^{-1}): 320 (0.64), 412 (0.17). MS (MALDI-TOF) *m/z*: 1688.3 (M^+).

[(adt)Ni(μ-tpbz)Ni(adt)], **17**. A 25 mL Schlenk flask with stir bar was charged with [Cl$_2$Ni(μ-tpbz)NiCl$_2$] (0.128 g, 0.12 mmol), [(adt)SnMe$_2$] (0.100 g, 0.24 mmol) and dry CH_2Cl_2 (15 mL). The resulting mixture was stirred for 12 h at 25 °C under N_2, during which time the insoluble [Cl$_2$Ni(μ-tpbz)NiCl$_2$] completely dissolved and a homogeneous dark brown solution resulted. This solution was reduced to dryness under vacuum, and the resulting brown solid residue was washed with MeOH (3 × 5 mL) followed by Et$_2$O (3 × 5 mL). Yield: 0.127 g, 70%. ^{1}H NMR (δ, ppm in CD_2Cl_2): 7.43-7.35 (m, 26H, aromatic C-*H*), 7.25-7.21 (m, 16H, aromatic C-*H*), 6.94 (d, 8H, *J* = 8.6 Hz, aromatic C-*H*), 6.51 (d, 8H, *J* = 8.6 Hz, aromatic C-*H*), 3.60 (s, 12H,
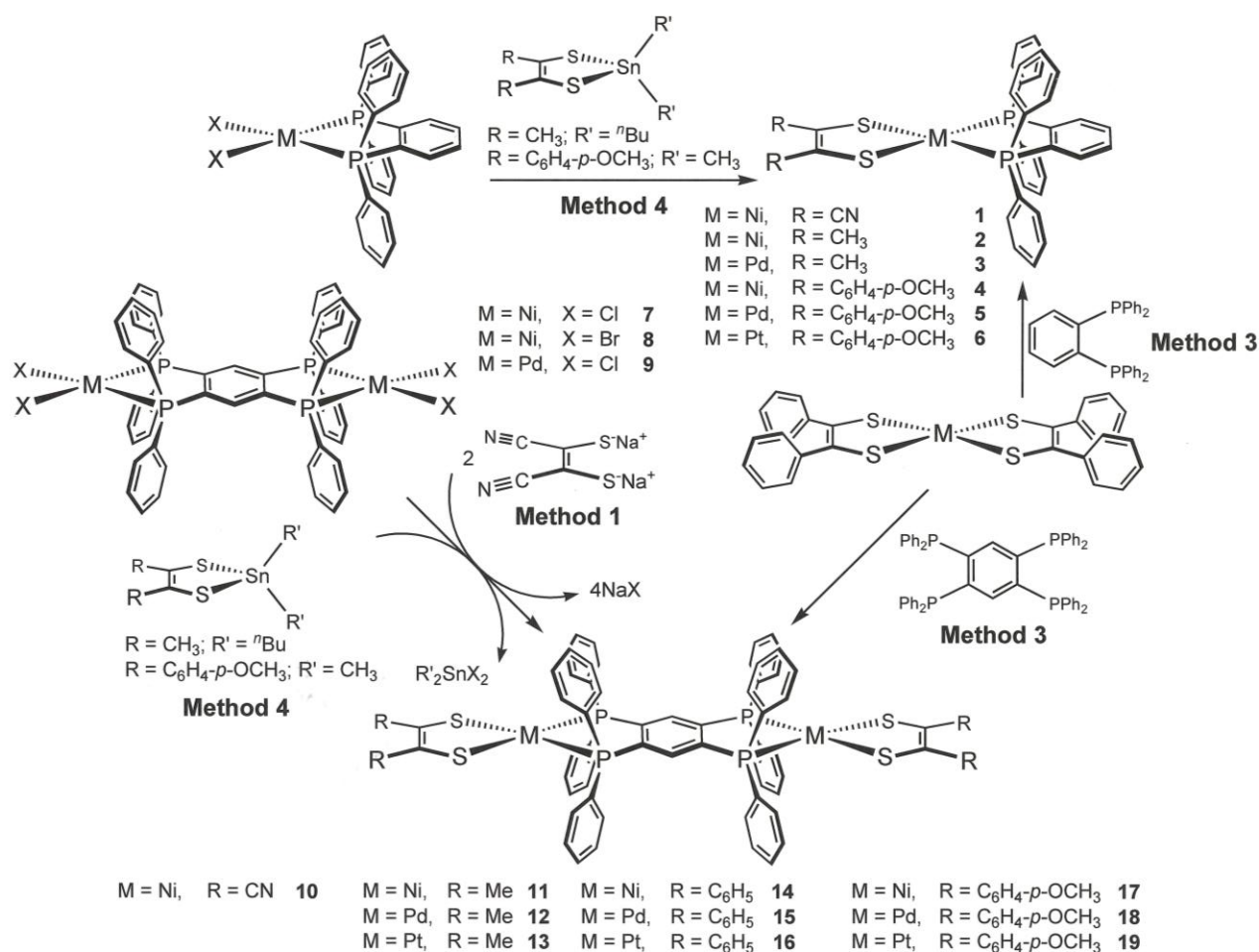
Scheme 2. Synthesis of monometallic dppb and dimetallic tpbz compounds.

dithiolene –OCH_3). ^{13}C NMR (δ, ppm in CD$_2$Cl$_2$): 157.9, 147.7, 135.3, 133.7, 131.4, 130.9, 129.7, 128.9, 112.9, 55.2. ^{31}P NMR (δ, ppm in CD$_2$Cl$_2$): 54.12. UV-vis (CH$_2$Cl$_2$), λ$_{max}$ nm (ε, 10^4 M^{-1} cm^{-1}): 314 (sh, 6.76), 484 (0.46), 640 (0.14). MS (MALDI-TOF) m/z: 1536.5 (M$^+$). Anal. Calcd for C$_{86}$H$_{70}$Ni$_2$O$_4$P$_4$S$_4$: C, 67.20; H, 4.59; P, 8.06. Found: C, 66.99; H, 4.79; P, 7.76.

[(adt)Pt(μ-tpbz)Pt(adt)], **19**. The same procedure and scale employed for the synthesis of **17** above were used but with [Cl$_2$Pt(μ-tpbz)PtCl$_2$] used in place in the corresponding nickel compound. Yield: 0.165 g, 76%. ^{1}H NMR (δ, ppm in CD$_2$Cl$_2$): 7.72-7.70 (m, 2H, aromatic C-H), 7.53-7.44 (m, 24H, aromatic C-H), 7.36-7.32 (m, 16H, aromatic C-H), 7.02 (d, 8H, J = 8.2 Hz, aromatic C-H), 6.59 (d, 8H, J = 8.4 Hz, aromatic C-H), 3.68 (s, 12H, dithiolene –OCH_3). ^{13}C NMR (δ, ppm in CD$_2$Cl$_2$): 158.0, 150.0, 136.3, 133.6, 131.8, 131.2, 129.1, 128.9, 112.9, 55.0. ^{31}P NMR (δ, ppm in CD$_2$Cl$_2$): 41.83 (s, J_{Pt-P} = 2738 Hz). UV-vis (CH$_2$Cl$_2$), λ$_{max}$ nm (ε, 10^4 M^{-1} cm^{-1}): 248 (sh, 1.19), 320 (sh, 2.73), 474 (0.55). MS (MALDI-TOF) m/z: 1809.3 (M$^+$).

(1)　　　$[(PR'_3)_2MCl_2] + Na_2(S_2C_2R_2) \longrightarrow [M(S_2C_2R_2)(PR'_3)_2] + 2NaCl$　　**Method 1**

(2)　　　$[Ni(CO)_2(PPh_3)_2] + \underset{F_3C}{\overset{S-S}{\underset{}{C=C}}}\underset{CF_3}{} \longrightarrow [Ni(S_2C_2(CF_3)_2)(PPh_3)_2] + 2CO$　　**Method 2**

(3)　　　$[M(S_2C_2R_2)_2] + 2PR'_3 \longrightarrow [M(S_2C_2R_2)(PR'_3)_2] + "S_2C_2R_2"$　　**Method 3**

(4)　　$[(PR'_3)_2MCl_2] + [R^*_2Sn(S_2C_2R_2)] \longrightarrow [M(S_2C_2R_2)(PR'_3)_2] + R^*_2SnCl_2$　　**Method 4**
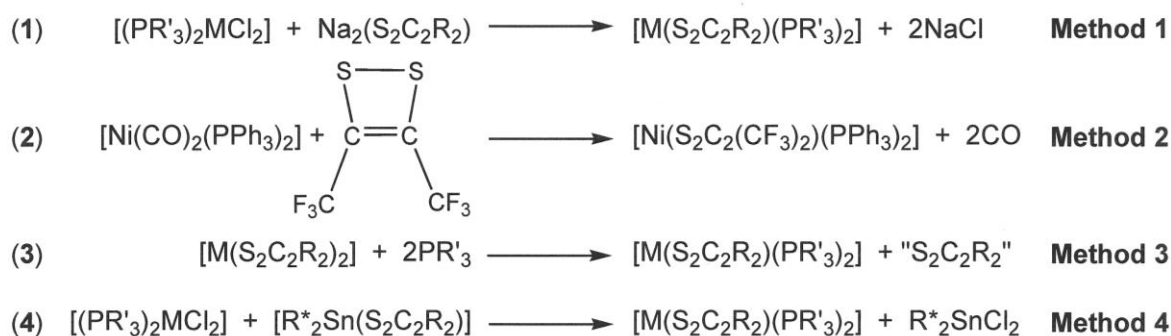
Physical Methods: UV-vis spectra were obtained at ambient temperature with a Hewlett-Packard 8452A diode array spectrometer, while IR spectra were taken as pressed KBr pellets with a Thermo Nicolet Nexus 670 FTIR instrument in absorption mode. All NMR spectra were recorded at 25 °C with a Varian Unity Inova spectrometer operating at 400, 100.5, and 161.8 MHz for ^{1}H, ^{13}C and ^{31}P nuclei, respectively. Spectra were referenced to the solvent residual. X-band EPR spectra were recorded on a Bruker ELEXSYS E500 spectrometer. The S-band EPR spectrum was measured on a Bruker ESP 300 spectrometer. Simulations were performed with XSophe[30] distributed by Bruker Biospin GmbH. Mass spectra (MALDI-TOF) were obtained with either an ABI Voyager-DE STR instrument or with a Bruker Autoflex III instrument operating in positive ion mode. Electrochemical measurements were made with a CHI620C electroanalyzer workstation using a Ag/AgCl reference electrode, a platinum disk working electrode, Pt wire as auxiliary electrode, and [^{n}Bu$_4$N][PF$_6$] as the supporting electrolyte. Under these conditions, the Cp$_2$Fe$^+$/Cp$_2$Fe (Fc$^+$/Fc) couple consistently occurred at +0.54 V in CH$_2$Cl$_2$ and at +0.48 V in *N,N*-dimethylformamide. Elemental analyses were performed by Midwest Microlab, LLC of Indianapolis, IN.

Results and Discussion

Syntheses. The period of intense, exploratory reactivity that marked the early beginnings of metallodithiolene chemistry as a subfield of coordination chemistry included reports of the preparation of monodithiolene bis(phosphine) complexes of the group 10 metals, the first heteroleptic dithiolene complexes, by several different routes. Holm and coworkers reported [(mnt)Ni(PPh$_3$)$_2$] and [(tfd)Ni(PPh$_3$)$_2$] (tfd = *cis*-1,2-dithio-1,2-bis(trifluoromethyl)ethylene) by substitution of halide from [NiCl$_2$(PPh$_3$)$_2$] (Eq. 1) and by oxidative addition of tfd (as 1,2-dithiacyclobutene) to [Ni(CO)$_2$(PPh$_3$)$_2$] (Eq. 2).[31] Shortly thereafter, Schrauzer and Mayweg

12

reported the synthesis of $[(S_2C_2R_2)M(PPh_3)_2]$ (M = Pd, Pt; R = Ph; M = Pt, R = Me) by displacement of dithiolene from $[M(S_2C_2R_2)_2]$ complexes (Eq. 3) to be an effective method of synthesis for this compound type.[32] Somewhat later, dialkyl tin dithiolene compounds, $R_2Sn(S_2C_2R'_2)$, were found to be effective transmetallating agents for delivery of a dithiolene ligand to $[MX_2(PR_3)_2]$ (X = halide) in exchange for the two eq. of halide (Eq. 4).[14,22,33-36]

The dppb and tpbz ligands are readily generated from 1,2-difluorobenzene and 1,2,4,5-tetrafluorobenzene by treatment with Na/PPh$_3$ in liquid NH$_3$. In one instance, the latter ligand was found to be adulterated with appreciable amounts of 1,4-bis(diphenylphosphino)-2,5-difluorobenzene, which was identified by X-ray crystallography (Figure S1). However, when this mixture was subjected to an additional treatment of Na/PPh$_3$ in NH$_3$, complete transformation to tpbz was observed. Isolation of pure tpbz is very much assisted by its modest solubility in CH$_2$Cl$_2$, which is effective in extracting and removing minor amounts of impurities.

The tetrahalide compounds **7**–**9** were readily prepared by procedures analogous to those employed for their mono-metallic counterparts. They are lightly colored and defined chiefly by their poor solubility, which is a consequence of their centrosymmetry and the surfeit of phenyl groups. They are modestly soluble in strongly polar solvents such as *N,N*-dimethylformamide and nitrobenzene, from which they tend to deposit crystals upon standing.

The synthetic approaches typified in Equations 3 and 4, designated hereafter as Methods 3 and 4, have been applied in the current work. Each approach bears advantages that render it preferable in particular situations, and each similarly suffers a shortcoming. Method 3 is desirable with $[M(S_2C_2R_2)_2]$ compounds (M = Ni, Pd or Pt; R = alkyl or aryl) that can be obtained in good yields directly in one step from P$_4$S$_{10}$, the corresponding α-hydroxyketone, and a source of M^{2+}. The practicality of this approach hinges upon the accessibility of the corresponding α-hydroxyketone. While fewer overall steps are involved, Method 3 can require column chromatography purification to separate modest amounts of the open-ended compounds, $[(S_2C_2R_2)M(\eta^2\text{-tpbz})]$. When applied in the synthesis of **14**, **15**, and **16**, Method 3 afforded yields in the range 60-89% for the intended dimetallic compound. Initial preparations of **16** by Method 3 were also attended by the minor amounts of the six-coordinate octahedral compound $[(pdt)_2Pt(\eta^2\text{-tpbz})]$, which was identified by X-ray crystallography. This compound type has been observed in earlier studies[20] of $[Pt(S_2C_2R_2)_2]$ with mono- and bidentate phosphines and found to be thermally susceptible to elimination of dithiolene ligand to afford the square planar
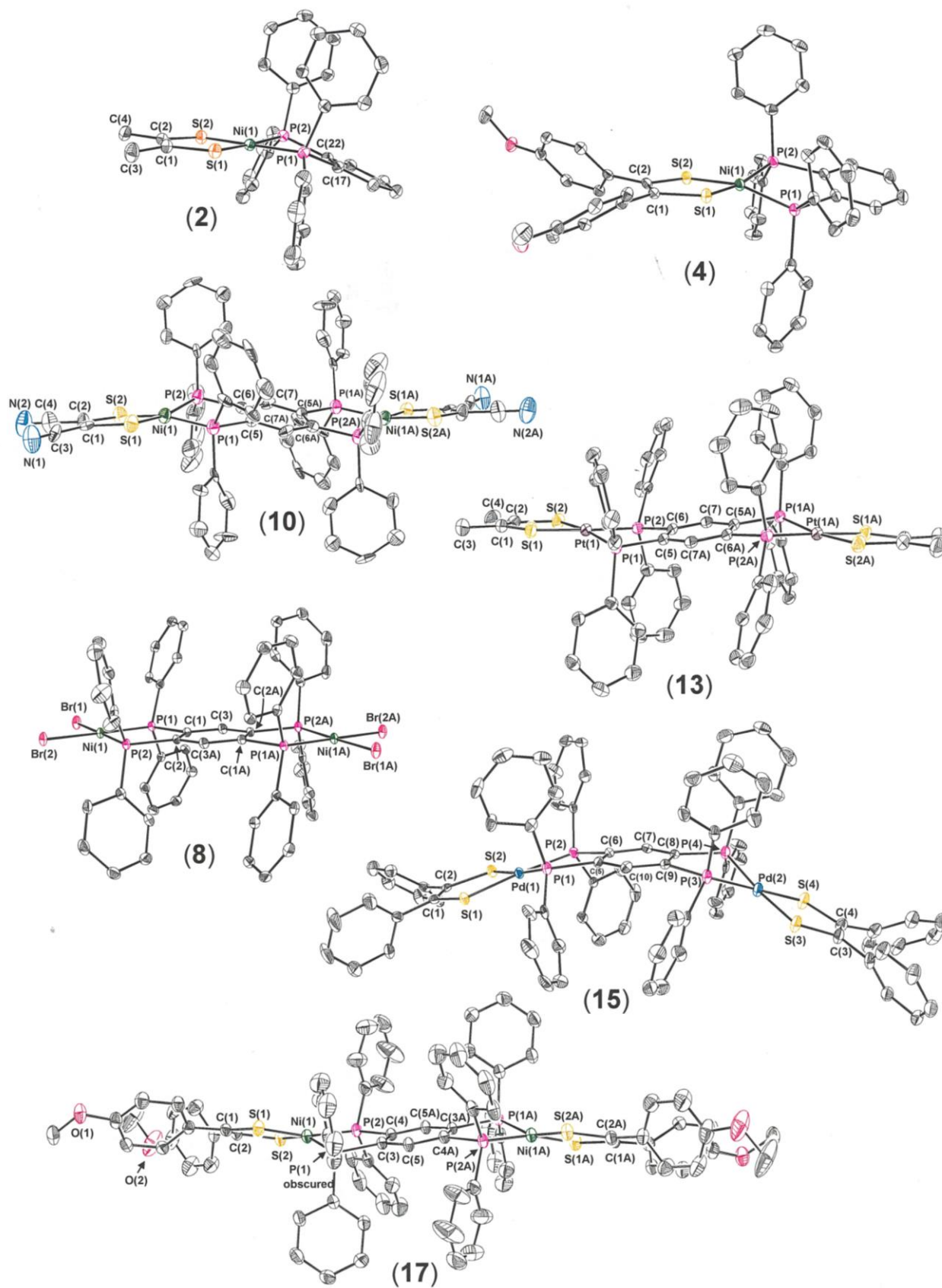
Figure 3. Thermal ellipsoid plots at the 50% probability level for selected compounds **2**, **4**, **8**, **10**, **13**, **15**, and **17**. Hydrogen atoms are omitted for clarity.

monodithiolene bis(phosphine) complex. The appearance of this intermediate [(pdt)$_2$Pt(η^2-tpbz)] is avoided by application of moderate warming and longer reaction times. More complete characterization of [(pdt)M(η^2-tpbz)] and [(pdt)$_2$Pt(η^2-tpbz)], as well as an account of their deployment toward further synthetic ends, are deferred to a later report.

Method 4, in our hands, supports the cleanest reactivity and highest percentage yields, making it preferred in reactions with the more expensive noble metals. Facile separation of the R′$_2$SnX$_2$ byproduct by straightforward washing with MeOH and Et$_2$O is another noteworthy expedience of this approach. The chief disadvantage of Method 4 is the series of additional synthesis steps demanded for access to the transmetallating agent, [(S$_2$C$_2$R$_2$)SnR′$_2$]. Method 4 has been applied in the synthesis of the mdt compounds **11**–**13** and the adt compounds **17**–**19** (Scheme 2), with the typical yield occurring in the range 70-80%. Compound **10** was prepared originally by Method 1, but its marginal solubility made effective purification difficult; subsequent preparations via Method 4 afforded cleaner samples in higher yields. Compounds **1**–**5** were readily prepared by Method 4 (Scheme 2) while, in the case of **6**, Method 3 was employed. The synthesis and physical characterization of these monometallic compounds were undertaken to provide guidance in interpreting the properties of the dimetallic congeners. Although compounds of the general type have been known, relatively few examples[9,37] with the dppb ligand have been described. All of these monometallic compounds are lightly colored and enjoy good solubility in chlorinated solvents such as CH$_2$Cl$_2$.

Structures. Crystal and refinement data for 1,4-(Ph$_2$P)$_2$-2,5-F$_2$-C$_6$H$_2$ (Table S1) and for the monometallic and dimetallic compounds of Scheme 2 are summarized in the supporting information (Tables S2 and S3-S6, respectively). These tables include data for additional crystal forms of **4**, **7** and **17**. Collectively, these data reveal a striking tendency for the dimetallic compounds to crystallize in monoclinic space group *P*2$_1$/*c* or its alternative setting *P*2$_1$/*n*. More often than not, the center of the tpbz ligand coincides with an inversion center such that half of the molecule is unique. Compound **12** differs from all the others by residing upon both a *C*$_2$ axis and an inversion center, which results in only one fourth of the molecule being crystallographically unique. Although the idealized point group for all the dimetallic compounds is *D*$_{2h}$, only **8** and **9** reveal a close adherence to this symmetry. Figure 3 illustrates thermal ellipsoid plots of selected representative compounds, a complete set of images with full atomic labeling being deferred to the supporting information (Figures S1-S55). Key metal-ligand and

Table 1. Selected interatomic distances, bond angles, and other structural parameters for compounds **1**–**5** and **7-9**. Averaged[a] values are given where two or more chemically identical interatomic distances or angles are present.

	1	2	3	4[i]	4[j]	5	7[k]	7[l]	8	9
M−X[b,c]	2.1544[7]	2.1476[4]	2.2901[3]	2.1483[4]	2.1463[4]	2.2938[4]	2.1945[5]	2.1996[5]	2.3287[2]	2.3503[5]
M−P[b]	2.1670[6]	2.1498[4]	2.2634[3]	2.1508[5]	2.1446[4]	2.2665[4]	2.1390[5]	2.1394[5]	2.1411[4]	2.2203[5]
Δ[d]	0.0126	0.0022	-0.0267	0.0025	-0.0017	-0.0273	-	-	-	-
S−C	1.739[3]	1.7567[14]	1.7662[13]	1.760[2]	1.7641[14]	1.7669[13]	–	–	–	–
$_S$C=C$_{-S}$	1.360(5)	1.336(3)	1.332(3)	1.360[3]	1.359(3)	1.353(3)	–	–	–	–
P−C$_{chelate}$	1.820[2]	1.8255[13]	1.8267[11]	1.828[2]	1.8254[14]	1.8252[13]	1.825[2]	1.821[1]	1.8266[13]	1.829[1]
$_P$C=C$_{-P}$	1.389(5)	1.398(3)	1.398(2)	1.396[3]	1.396(3)	1.397(3)	1.394(4)	1.392(3)	1.401(3)	1.392(3)
M···M[b]	–	–	–	–	–	–	8.738	8.709	8.741	8.857
md,[e] Å	0.0875	0.0308	0.0699	0.2186	0.2340	0.0468	0.0981	0.1057	0.0250	0.0617
δ,[f] Å	0.0121	0.0219	0.0221	0.0188	0.0353	0.0079	0.0234	0.0038	0.0008	0.0230
X−M−X[b,c]	93.07(4)	91.57(2)	88.396(16)	91.59[2]	91.64(1)	88.604(17)	94.73(3)	95.80(2)	94.968(11)	93.83(2)
P−M−P[b]	87.52(3)	86.01(2)	85.849(15)	88.92[2]	88.68(2)	86.032(18)	89.24(3)	89.06(2)	89.03(2)	87.70(2)
X−M−P$_{cis}$[b,c]	89.98[3]	91.22[1]	93.009[1]	91.53[2]	91.80[1]	92.751[12]	88.33[2]	87.99[1]	88.023[11]	89.33[1]
X−M−P$_{trans}$[b,c]	173.69[3]	176.42[1]	175.630[11]	165.55[2]	164.72[1]	176.853[12]	173.18[2]	172.28[2]	176.590[13]	175.25[1]
θ,[g] deg.	8.1	3.2	6.3	20.4	21.8	4.2	8.9	9.6	2.2	5.5
φ,[h] deg.	12.8	24	13.1	8.6	0.70	14.5	2.7	3.7	3.3	3.3

[a]Uncertainties are propagated according to Taylor, J. R. *An Introduction to Error Analysis*; 2nd ed.; University Science Books: Sausalito, CA, 1997, pp 73-77. [b]M= Ni, Pd or Pt. [c]X = S, Cl or Br. [d]Δ = M–P$_{ave}$ – M–S$_{ave}$. [e]md = mean atom deviation (Å) from X$_2$MP$_2$ plane. [f]δ = deviation (Å) of M from X$_2$MP$_2$ plane. [g]Angle between S$_2$M and P$_2$M planes. [h]Angle between MP$_2$ and P$_2$C$_6$ mean plane. [i]Values are from structure determination of **4** without interstitial solvent. [j]Values are from structure determination of **4** with 2 CH$_2$Cl$_2$ interstitial solvent molecules. [k]Values are from structure determination of **6** with 2 CHCl$_3$ interstitial solvent molecules. [l]Values are from structure determination of **6** with 4 DMF interstitial solvent molecules.

Table 2. Selected interatomic distances, bond angles, and other structural parameters for compounds **10–19**. Averaged[a] values are given where two or more chemically identical interatomic distances or angles are present.

	10	11	12	13	14	15	16	17[h]	17[i]	18[j]	19[k]
M–S[b]	2.157[2]	2.1503[5]	2.287(2)	2.2975[7]	2.1367[6]	2.2908[8]	2.2929[8]	2.1492[5]	2.1435[4]	2.2858[5]	2.291[3]
M–P[b]	2.167[2]	2.1598[4]	2.265(2)	2.2439[7]	2.1487[6]	2.2618[9]	2.2487[8]	2.1628[5]	2.1641[4]	2.2709[5]	2.248[3]
Δ[c]	+0.010	+0.0095	-0.022	-0.0536	+0.012	-0.0290	-0.0442	+0.0136	+0.0206	-0.0149	-0.043
S–C	1.750[7]	1.764[2]	1.757(8)	1.768[3]	1.753[3]	1.760[3]	1.761[3]	1.760[2]	1.759[1]	1.771[2]	1.768[11]
$_S$C=C$_S$	1.356(13)	1.335(4)	1.350(19)	1.344(6)	1.334(4)	1.339[6]	1.347[7]	1.357[4]	1.352(3)	1.348[4]	1.33(2)
P–C$_{chelate}$	1.811[6]	1.831[1]	1.819(6)	1.825[3]	1.832[2]	1.841[3]	1.823[3]	1.832[2]	1.825[1]	1.827[2]	1.822[10]
$_P$C=C$_P$	1.422(11)	1.401(3)	1.426(12)	1.400(5)	1.400(6)	1.395[6]	1.403[6]	1.404[4]	1.401(3)	1.397[3]	1.39(2)
M···M[b]	8.757	8.738	8.875	8.862	8.746	8.671	8.848	8.711	8.689	8.822	8.766
md,[d] Å	0.1887	0.1073	0.0068	0.0766	0.0399, 0.2169	0.0785, 0.0588	0.0329, 0.0737	0.2554, 0.2496	0.2554	0.0958	-[l]
δ,[e] Å	0.0102	0.0491	0.0169	0.0483	0.0116, 0.0249	0.0118, 0.0301	0.0197, 0.0165	0.0189, 0.0496	0.0418	0.0319	-[l]
S–M–S	93.28(12)	91.09(3)	87.94(11)	88.29(4)	90.59(3)	89.00[4]	88.90[4]	91.47[3]	91.46(2)	88.80[3]	88.97(14)
P–M–P	88.59(11)	88.48(3)	87.17(9)	86.76(3)	89.12(3)	85.82[4]	87.30[2]	89.17[3]	89.57(2)	85.23[3]	84.52(14)
S–M–P$_{cis}$	90.40[8]	90.50[1]	92.44(7)	92.57[3]	90.19[2]	92.73[3]	91.99[3]	91.93[2]	91.78[1]	93.34[2][m]	96.81(14)
S–M–P$_{trans}$	167.35[8]	173.37[2]	178.87(9)	175.64[2]	177.37[3]	175.16[3]	176.21[3]	163.54[3]	163.47[2]	173.41[2][n]	176.42(16)
θ,[f] deg.	17.5	10.3	1.5	7.3	3.7, 20.3	7.0, 5.5	3.2, 6.6	23.8, 23.1	23.7	9.0[o]	-[l]
φ,[g] deg.	9.8	13.3	11.3	13.3	5.2, 3.9	14.9, 29.0	12.3, 11.5	11.1, 15.2	13.0	23.2[p]	-[l]

[a]Uncertainties are propagated according to Taylor, J. R. *An Introduction to Error Analysis*; 2nd ed.; University Science Books: Sausalito, CA, 1997, pp 73-77. [b]M= Ni, Pd or Pt. [c]Δ = M−P$_{ave}$ − M−S$_{ave}$. [d]md = mean atom deviation from X$_2$MP$_2$ plane. [e]δ = deviation (Å) of M from X$_2$MP$_2$ plane. [f]Angle between S$_2$M and P$_2$M planes. [g]Angle between MP$_2$ and P$_2$C$_6$ mean plane. [h]Values are for structure determination of **16** with 1,2-dichloroethane interstitial solvent. [i]Values are for structure determination of **16** without interstitial solvent. [j]Values are averages for 3 independent whole molecules and 2 independent half-molecules in the asymmetric unit of the unit cell. [k]Values are taken from two separate half-molecules in the asymmetric unit of the cell from only those parts of the molecules which were not disordered. [l]No meaningful value can be assessed owing to static disorder in the molecule. [m]Values range from 89.46(9) − 98.13(8)°. [n]Values range from 166.68(8) − 177.96(8)°. [o]Values range from 3.2 − 15.7°. [p]Values range from 13.5 − 29.8°.

Table 3. Comparison of measured M–S and M–P bond lengths for [(pdt)M(μ-tpbz)M(pdt)] against calculated M–S and M–P bond lengths in [(pdt)M(dppb)] (M = Ni, Pd, or Pt).

	Expt., **14**	Calc., M = Ni	Expt., **15**	Calc., M = Pd	Expt., **16**	Calc., M = Pt
M–S$_{ave}$	2.1367[6]	2.2017	2.2908[8]	2.3420	2.2929[8]	2.3560
M–P$_{ave}$	2.1487[6]	2.2585	2.2618[9]	2.3565	2.2487[8]	2.3277
Δ^a	-0.012	-0.0568	+0.029	-0.0145	+0.0442	+0.0283

^{a}Δ = (M–S$_{ave}$) – (M–P$_{ave}$).

intraligand bond lengths and angles, presented where possible as averaged values, are shown in Tables 1 and 2. Dithiolene C–S and C–C$_{chelate}$ bond lengths are, in all cases, indicative of the fully reduced ene-1,2-dithiolate(2–) redox form the of the dithiolene ligand. The metal ions in all compounds are thus divalent cations.

The bis(halide) tpbz compounds **8**–**9** show distinctly planar configurations. In contrast, modest distortions from planarity are readily apparent in the dithiolene compounds, although the coordination geometries about the metal ions are closer to the square planar ideal than otherwise. Gauged as the angle, θ, between S$_2$M and P$_2$M planes, the observed distortion angles are somewhat greater for the Ni compounds than for the analogous Pd and Pt complexes (Tables 1 and 2). The greatest value of θ, 23.8° is found for **17**. Considering the compounds as a whole set, the distortion is as pronounced for the dimetallic dithiolene compounds as it is for the monometallic analogues. This greater tendency for square planar coordination by Pd and Pt, as compared to Ni is a general phenomenon and attributed to the greater ligand field stabilization experienced by the heavier metals.[38] Examination of the mono(dithiolene) bis(phosphine) complexes of the group 10 metals occurring in the Cambridge Structural Database shows a
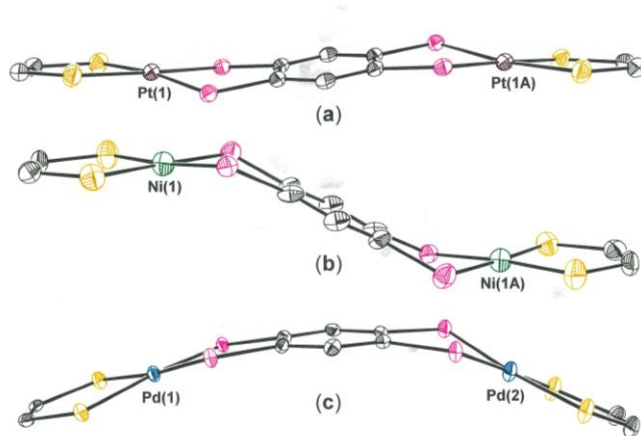

Figure 4. Core topology of (a) diplatinum compound **13**, (b) one of several crystal forms of dinickel compound **17**, and (c) dipalladium compound **15**. Image (b), from a form of **17** with disordered interstitial C$_6$H$_5$Cl, has values of 4.4° for θ and 30.7° for φ.

similar proclivity for distortion among the Ni compounds and greater adherence to the square planar ideal among Pd and Pt complexes.

A second form of distortion in the dimetallic dithiolene compounds is a folding of the tpbz along the axes defined by two chelating phosphorus atoms such that the S_2MP_2 mean plane meets the P_2C_6 mean plane at a nonzero angle. These fold angles, φ, are shown in Tables 1 and 2 for all compounds. Because the tpbz fold angle does not disrupt planarity in the immediate environment of the metal atom, it occurs with a magnitude and frequency unrelated to the identity of the metal atom. The consequence of twisting of the S_2M plane relative to the MP_2 plane in conjunction with the folding within the bridging tpbz ligand is a surprising diversity of conformation among these dimetallic compounds. They may appear as gently undulating (Figure 4a), as folded into a "chair" conformation (Figure 4b), or bowed into a "boat" conformation (Figure 4c). The slightly varying distance between metal ions in these dimetallic compounds (Table 1) reflects these variable conformations. These distorted static structures in the crystalline state undoubtedly reflect packing forces and are not anticipated to be important in the solution phase even though they might be transiently sampled.

A pattern that emerges from the structural data in Tables 1 and 2 for the nickel dithiolene bis(phosphine) compounds is an average Ni–S bond length that is consistently ~0.01 Å *shorter* than the averaged Ni–P bond length (*cf.* Tables 1 and 2, 3rd row). This difference is significant within the resolution of the data. In isostructural compounds with M = Pd and Pt, however, M–S_{ave} *exceeds* M–P_{ave} by margins of ~0.02 Å and ~0.045 Å, respectively. Contrast, for example, the third row entries for **15** and **16** against that for **14** (Table 2). This variation in differences of metal ligand bond lengths as function of metal is evident in related series of group 10 compounds whose crystal structures are available for comparison[10,11,39,40] but, heretofore, has not drawn notice.

To assess the changing MO compositions that likely underpin these changing differences in M−S_{ave} and M−P_{ave} bond lengths, gas phase optimizations were undertaken of [(pdt)M(dppb)] (M = Ni, Pd, Pt) by DFT at the B3LYP level of theory with typical basis sets. Table 3 summarizes optimized bond lengths and compares them with the corresponding averaged values from dimetallic tpbz-bridged compounds **14**–**16**. Optimized metal-ligand bond lengths systematically exceed experimentally determined values by ~0.1 Å, as is typically found with the B3LYP functional.[41] Notably, the trend in Δ, the difference between M−S_{ave} and M−P_{ave} is

Table 4. Percentage contribution to highest occupied MOs in [M(pdt)(dppb)] (M = Ni, Pd, Pt) by M, sulfur, and phosphorus, as determined by Mulliken population analysis.[a] Colored type identifies the key MOs that have qualitatively similar composition.

	[Ni(pdt)(dppb)]		[Pd(pdt)(dppb)]		[Pt(pdt)(dppb)]	
	Fragment	% Contrib.	Fragment	% Contrib.	Fragment	% Contrib.
HOMO $M\,d - S\,p\,\pi^*$	Ni	7.3	Pd	6.0	Pt	6.7
	S	41.7	S	45.9	S	44.9
	P	1.9	P	1.6	P	2.0
HOMO-1 $M\,d - S\,p\,\pi^*$	Ni	17.8	Pd	11.1	Pt	15.2
	S	61.6	S	66.2	S	63.6
	P	0.1	P	0.2	P	0.4
HOMO-2 $M\,d - S\,p\,\sigma$	Ni	12.0	Pd	6.9	Pt	6.8
	S	18.6	S	17.1	S	15.3
	P	3.1	P	4.2	P	3.3
HOMO-3 $M\,d - S\,p\,\sigma$	Ni	**70.6**	Pd	**23.3**	Pt	**2.2**
	S	**16.7**	S	**31.7**	S	**11.2**
	P	~0	P	1.1	P	4.6
HOMO-4 $M\,d - S\,p\,\sigma$	Ni	**4.6**	Pd	**4.4**	Pt	**13.1**
	S	**20.6**	S	**16.7**	S	**10.8**
	P	5.7	P	6.8	P	0.9
HOMO-5 $M\,d - S\,p$	Ni	**17.1**	Pd	**24.5**	Pt	**63.0**
	S	**3.0**	S	**18.1**	S	**13.4**
	P	0.7	P	0.4	P	1.6

[a]Mulliken population analysis performed with QM Forge.

replicated in the calculations. A shorter $M-S_{ave}$ than $M-P_{ave}$ is calculated for the nickel compound, and this difference narrows for [(pdt)Pd(dppb)]. For [(pdt)Pt(dppb)], the magnitude of $M-S_{ave}$ overtakes $M-P_{ave}$, but in the experimental data this crossover occurs with M = Pd.

A visual inspection of the highest occupied MOs across the [(pdt)M(dppb)] (M = Ni, Pd, Pt) series, in conjunction with a Mulliken population analysis that provides the percentage contribution to these MOs by the metal d, sulfur p and phosphorus p atomic orbitals, shows both the HOMO and HOMO-1 to be $M\,d - S\,p\,\pi^*$ MOs with essentially the same composition across the series (Table 4, Figures S56-S58). Several of the deeper lying MOs, however, change appreciably in the relative contributions of M d and S p orbitals across the series while still maintaining qualitative similarity (Table 4). The HOMO-3 for both [(pdt)Ni(dppb)] and [(pdt)Pd(dppb)], are comprised of $M\,d_{z^2}$ and of S p orbitals that are canted modestly above and below the chelate plane such that slight positive overlap occurs between them and the lobes of the d orbital that are likewise above and below the S_2MP_2 plane (Figure 5). The corresponding MO in [(pdt)Pt(dppb)] (HOMO-4) is greatly diminished in both M d and S p character, and no
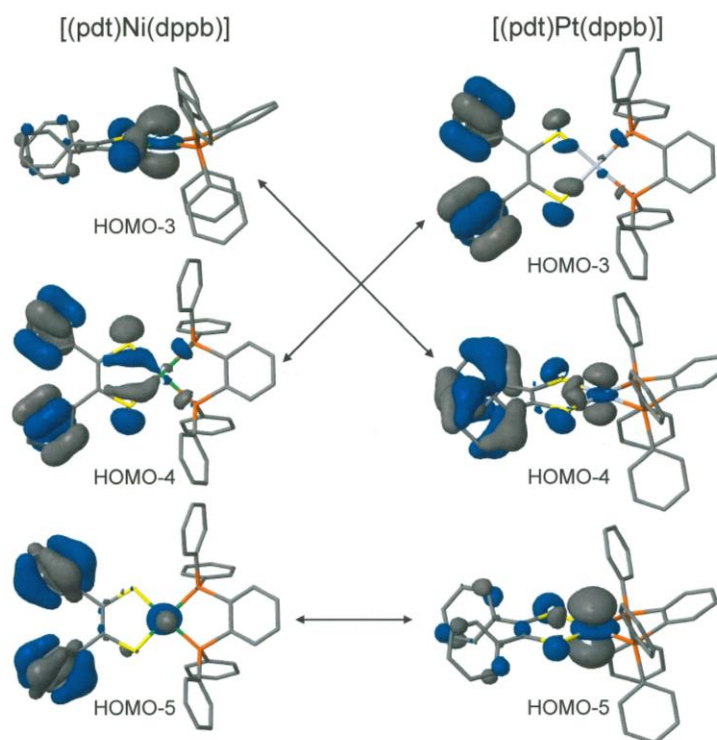
Figure 5. Filled MOs HOMO-3 through HOMO-5 for [(pdt)Ni(dppb)] (left) and [(pdt)Pt(dppb)] (right). For the platinum compound, diminished M d – S p σ character is evident in the HOMO-3 and HOMO-4, relative to the Ni compound, and greater σ* character is present in the HOMO-5. The orbital images are presented at the 0.035 contour level.

effective overlap occurs between them. The HOMO-4 in [(pdt)Ni(dppb)] and [(pdt)Pd(dppb)] has minor M d – S p σ-character (Figure 5), but its counterpart in [(pdt)Pt(dppb)] (HOMO-3) has almost no contribution from metal at all. The HOMO-5 for [(pdt)Ni(dppb)] has modest d_{z2} character (~17%) and almost no contribution from sulfur p orbitals. The HOMO-5 in [(pdt)Pt(dppb)] is greater in both metal d (~63%) and sulfur p (~13%) contributions, the interaction between which is σ*. Thus, the cumulative effect of attenuated metal d – sulfur p σ overlap (HOMO-3, HOMO-4) and increased σ* character to the HOMO-5 induces lengthening of the Pd–S and Pt–S bonds to the extent that they exceed M–P bond lengths.

Electrochemistry. Monometallic compounds **1**–**6** and dimetallic compounds **10**–**19** display a rich redox chemistry (Figures S59-S87) which, in all cases except that for **1** and **10**, is ligand-based behavior. Compounds **11**–**19** sustain a reversible or quasireversible oxidation at ~0 V vs Fc$^+$/Fc, which is attributed to concurrent oxidation of the dithiolene end groups to radical monoanions: $[(R_2C_2S_2)M(\mu\text{-tpbz})M(S_2C_2R_2)] \rightarrow [(R_2C_2S^-S^\bullet)M(\mu\text{-tpbz})M(S^-S^\bullet C_2R_2)]^{2+} + 2e^-$

(a) **[{(adt)Ni}$_2$(μ-tpbz)]**, **17**

$E_{1/2}(1) = -2.05$ V
$E_{1/2}(2) = -0.04$ V
$E_{1/2}(3) = +0.49$ V

(b) **[(adt)Ni(dppb)]**, **4**

$E_{1/2}(1) = -0.15$ V
$E_{1/2}(2) = +0.44$ V

(c) **[{(mdt)Pd}$_2$(μ-tpbz)]**, **12**

$E_{1/2}(1) = -1.99$ V
$E_{1/2}(2) = -0.10$ V

(d) **[{(mnt)Ni}$_2$(μ-tpbz)]**, **10**

$E_{1/2}(1,2) = -1.35, -1.45$ V
$E_{1/2}(3,4) = -2.13, -2.34$ V

2 μA

Potential, Volts vs Fc$^+$/Fc
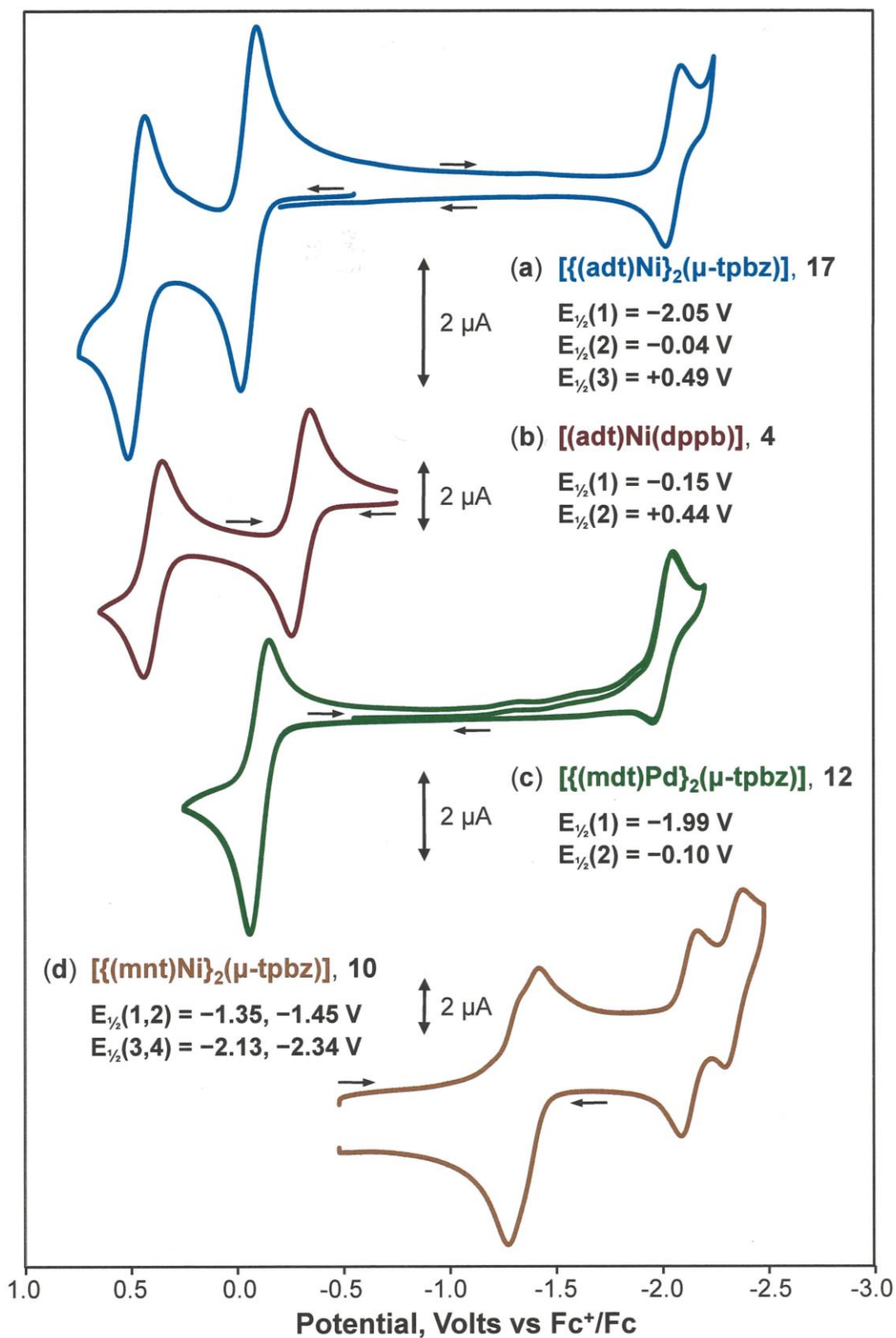
Figure 6. Cyclic voltammograms of representative tpbz-linked metallodithiolene compounds: (a), [(adt)Ni(μ-tpbz)Ni(adt)], in CH$_2$Cl$_2$; (c), [(mdt)Pd(μ-tpbz)Pd(mdt)], in CH$_2$Cl$_2$; (d) [(mnt)Ni(μ-tpbz)Ni(mnt)], in DMF. The voltmmogram of monometallic [(adt)Ni(dppb)], (b), provides reference for interpreting the dimetallic compounds.

(Figure 6). Confirmation of the $2e^-$ nature of the process arises from, *inter alia*, comparison of the current amplitude to that seen for the analogous process in monometallic [(adt)Ni(dppb)] and from charge counting in a bulk electrolysis experiment. The minor variance of the potential as the identity of the metal ion is changed while the ligand environment is constant is also consistent with ligand-based redox chemistry. The potential at which oxidation occurs is nearly the same for R = Me and R = *p*-anisyl, indicating similarity in the magnitude of the electron-donating effect of these two substituents. Since they are less electron-rich and therefore modestly less effective in supporting the positive charge upon oxidation, the R = Ph compounds show a modest anodic shift of ~0.10 V for this first oxidation relative to the R = *p*-anisyl compounds (Table 5). A point of contrast between the mdt compounds, **11**–**13**, and those with aryl substituents, **14**–**19**, is that the latter set supports a second reversible $2e^-$ oxidation in the range +0.49 – +0.79 V vs Fc^+/Fc while the former does not (Figure 6c vs Figure 6a). Potentials for the second oxidation in **11**–**13** were therefore obtained by differential pulse voltammetry (Figures S73, S76, S79). A possible reason for the reversibility supported by **14**–**19** is a somewhat greater steric profile cast above and below the ligand chelate by the arene rings, as they are invariably canted by ~30° relative to the MS_2C_2 mean plane and protect the inherently reactive dithione that is created upon the second $2e^-$ oxidation.

In the cathodic direction, a reversible reduction is observed for **11**–**19** at ~-2.0 V vs Fc^+/Fc that is assigned to reduction of the tpbz bridging ligand on the following collected bases: 1) The current amplitude is half that of the oxidation waves, indicating a $1e^-$ process arising from the unique fragment of these molecules; 2) The potential at which this reduction occurs is essentially invariant as both M and R are varied, indicating that it has a common assignment across **11**–**19**; 3) This feature is not observed in the cyclic voltammograms for the mono-metallic dppb compounds **1**–**6**; 4) A gas phase optimization of the geometry of **19** (Table S10) and inspection of its LUMO and LUMO+1 (Figure S88) show them to be localized on the tpbz bridging ligand.

The reversible oxidations found for **14**–**19** contrast sharply with the electrochemistry reported for a series of dipalladium and diplatinum compounds with arene-1,2-dithiolate end groups and two bridging 1,2-bis(diphenylphosphino)acetylene ligands (Figure 7).[42] Two irreversible oxidation waves were reported, the first attributed to the arene-1,2-dithiolate ligand. The irreversibility is likely the consequence of both poorer delocalization of the sulfur radical

Table 5. Electrochemical Data (in V vs. Fc⁺/Fc)

	E_2 (ox)	E_1 (ox)	E_3 (red)	Solvent, WE[a]
[(mdt)Ni(dppb)], **2**	+0.50 (ir)[b,c]	-0.20 (r, 1e)[d]	-	CH_2Cl_2, Pt disk
[(adt)Ni(dppb)], **4**	+0.44 (r, 1e)	-0.15 (r, 1e)	-	CH_2Cl_2, Pt disk
[(adt)Pd(dppb)], **5**	+0.40 (r, 1e)	-0.20 (r, 1e)	-	CH_2Cl_2, Pt disk
[(adt)Pt(dppb)], **6**	+0.53 (r, 1e)	-0.10 (r, 1e)	-	CH_2Cl_2, Pt disk
[(mdt)Ni(μ-tpbz)Ni(mdt)], **11**	+0.61 (ir)[b,c]	-0.03 (qr, 2e)[e]	-2.10 (qr, 1e)	CH_2Cl_2, Pt disk
[(mdt)Pd(μ-tpbz)Pd(mdt)], **12**	+0.68 (ir)[c]	-0.10 (qr, 2e)	-1.99 (qr, 1e)	CH_2Cl_2, Pt disk
[(mdt)Pt(μ-tpbz)Pt(mdt)], **13**	+0.75 (ir)[c]	-0.04 (r, 2e)	-2.07 (qr, 1e)	CH_2Cl_2, Pt disk
[(pdt)Ni(μ-tpbz)Ni(pdt)], **14**	+0.66 (r, 2e)	+0.07 (r, 2e)	-2.02 (r, 1e)	CH_2Cl_2, GC[f]
[(pdt)Pd(μ-tpbz)Pd(pdt)], **15**	+0.73 (r, 2e)	+0.02 (r, 2e)	-1.96 (r, 1e)	CH_2Cl_2, Pt disk
[(pdt)Pt(μ-tpbz)Pt(pdt)], **16**	+0.79 (r, 2e)	+0.09 (r, 2e)	-2.05 (r, 1e)	CH_2Cl_2, Pt disk
[(adt)Ni(μ-tpbz)Ni(adt)], **17**	+0.49 (r, 2e)	-0.04 (r, 2e)	-2.05 (qr, 1e)	CH_2Cl_2, Pt disk
[(adt)Pd(μ-tpbz)Pd(adt)], **18**	+0.50 (r, 2e)	-0.04 (r, 2e)	-1.97 (qr, 1e)	CH_2Cl_2, Pt disk
[(adt)Pt(μ-tpbz)Pt(adt)], **19**	+0.53 (r, 2e)	-0.02 (r, 2e)	-2.09 (qr, 1e)	CH_2Cl_2, Pt disk
	E_1 (red)	E_2 (red)	E_3 (red)	Solvent, WE[a]
[(mnt)Ni(dppb)], **1**	-1.43 (r, 1e)	-2.22 (r, 1e)	-	DMF, GC[f]
[(mnt)Ni(μ-tpbz)Ni(mnt)], **10**	-1.35, -1.45[g] (r, 1e, 1e)	-2.13 (r, 1e)	-2.34 (r, 1e)	DMF, GC[f]

[a]WE = Working electrode; [b]ir = irreversible; [c]Value obtained by differential pulse voltammetry; [d]r = reversible; [e]qr = quasireversible; [f]GC = glassy carbon. [g]Potentials estimated from differential pulse voltmmetry by width-at-half-height analysis as described by Richardson and Taube.[40]

across the dithiolene chelate as well as greater exposure of the ligand radical to other processes such as dimerization or decomposition induced by the supporting electrolyte. Other compounds of the type but with dithiolene ligands (**d**–**g**; Figure 7) sustain a single reversible oxidation of the dithiolene ligands in the same manner as **11**–**13**.[43]

The cyclic voltammogram for **10**, [(mnt)Ni(μ-tpbz)Ni(mnt)], is qualitatively very different from those of **11**–**19**. Owing to its poor solubility in CH_2Cl_2, the voltammetry for **10** had to be conducted in *N*,*N*-dimethylformamide. No reversible oxidation is supported by **10** due to the very electron-withdrawing nature of the cyano substituents of the dithiolene ligand. In the
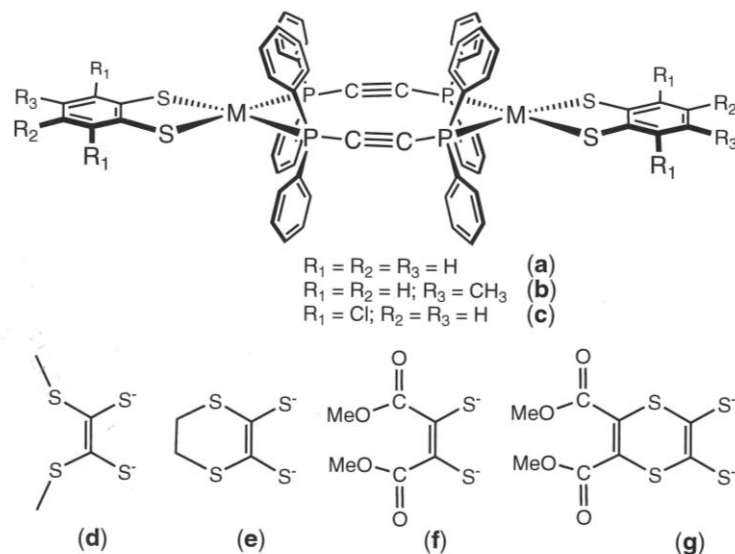
Figure 7. Dimetallic Pd and Pt compounds with 1,2-bis(diphenylphosphino)acetylene bridging ligands and dithiolene end groups.

cathodic direction, however, a feature is observed at ~-1 V that is obviously two highly overlapped and unresolved reduction waves occurring at close, but not identical, potentials (Figure 6d). The observations that the $(mnt)^{2-}$ ligand is fully reduced and that the potential for tpbz reduction occurs at somewhat more negative potentials in **11**–**19** suggest that these reductions be assigned as $Ni^{II} + e^- \rightarrow Ni^I$ processes. This assignment is plausible, as metal-based reduction has been noted previously in the dinickel compounds $[(dppb)Ni(\mu\text{-}tpbz)Ni(dppb)]^{4+}$,[44] $[(mnt)Ni(\mu\text{-}trans\text{-}dppee)Ni(mnt)]^{45}$ and $[(mnt)Ni(\mu\text{-}trans\text{-}dmpee)Ni(mnt)]^{45}$ (dppee = trans-1,2-di(phenylphosphino)ethylene, dmpee = trans-1,2-di(methylphenylphosphino)ethylene). Because the physical separation of Ni^{II} ions in **10** is appreciably smaller than the distance between the centroids of the redox-active dithiolene ligands in **11**–**19**, the onset of resolution between the two reduction processes is expected. Differential pulse voltammetry upon **10** (Figure S70) and analysis of the overlapped peaks by the width-at-half-height method described by Taube[46] provides an estimate of ~95 – 100 mV as the true separation between these successive reductions. At more reducing potentials, two additional reduction waves are observed at -2.13 and -2.34 V and assigned as successive $Ni^I + e^- \rightarrow Ni^0$ reductions (Figure 6d). The accumulation of negative charge manifests itself in greater separation between the third and fourth reductions even though they are attributable to otherwise identical processes. Corroboration of these assignments is found in the cyclic voltammogram of

25

Table 6. Electronic Absorption Data

Compound	λ_{max}, nm (ε, 10^4 M^{-1}, cm^{-1})
[(mnt)Ni(dppb)], **1**	~435 (sh, ~0.12), 550 (0.02)
[(mdt)Ni(dppb)], **2**	404 (0.23), 626 (0.02)
[(mdt)Pd(dppb)], **3**	369 (0.09), 403 (0.08), 545 (0.01)
[(adt)Ni(dppb)], **4**	~406 (sh, ~0.42), 618 (0.07)
[(adt)Pd(dppb)], **5**	~416 (sh, ~0.14), 548 (0.06)
[(adt)Pt(dppb)], **6**	~330 (sh, 0.50), 390 (0.21)
[Cl$_2$Ni(μ-tpbz)NiCl$_2$], **7**	460 (0.25)
[Br$_2$Ni(μ-tpbz)NiBr$_2$], **8**	476 (0.37)
[(mdt)Ni(μ-tpbz)Ni(mdt)], **11**	308 (sh, 2.49), 478 (0.23)
[(mdt)Pd(μ-tpbz)Pd(mdt)], **12**	268 (sh, 7.24), 484 (0.23)
[(mdt)Pt(μ-tpbz)Pt(mdt)], **13**	350 (sh, 0.49), 472 (0.35)
[(pdt)Ni(μ-tpbz)Ni(pdt)], **14**	376 (sh, ~0.67), 474 (0.29), 622 (0.07)
[(pdt)Pd(μ-tpbz)Pd(pdt)], **15**	480 (0.12)
[(pdt)Pt(μ-tpbz)Pt(pdt)], **16**	320 (0.66), 412 (0.19)
[(adt)Ni(μ-tpbz)Ni(adt)], **17**	270 (sh, 9.11), 314 (sh, 6.76), 484 (0.46), 640 (0.14)
[(adt)Pd(μ-tpbz)Pd(adt)], **18**	262 (sh, 10.6), 496 (0.35), ~600 (unresolved sh, 0.20)
[(adt)Pt(μ-tpbz)Pt(adt)], **19**	248 (sh, 1.19), 320 (sh, 2.73), 474 (0.55)

1 (Table 5), which reveals two highly reversible waves at -1.43 V and -2.22 V corresponding to the two sets of waves found for **10**. Furthermore, optimization of the geometry of **10** in DMF solution and inspection of its LUMO and LUMO+1 show that they may be characterized as essentially metal-ligand σ^* MOs involving the Ni d_{x2-y2} orbitals, although the LUMO has appreciable contribution from π-type MOs of the tpbz ligand as well (Table S11, Figure S89).

Electronic absorption spectra

Mononuclear compounds **4–6** show two features in the electronic absorption spectra below the onset of the $\pi \rightarrow \pi^*$ transitions of the arene rings in the 300 nm region. The higher energy feature is an unresolved shoulder in the 330 – 416 nm range, while the lower energy absorption spans a fairly broad energy range (390 – 618 nm, Table 6). A time-dependent DFT calculation of the electronic absorption spectrum of [(pdt)Ni(dppb)] shows its lowest energy excitation to be a HOMO (dithiolene C$_2$S$_2$ π system) $\rightarrow$ LUMO transition. The LUMO is the σ^* MO between Ni d_{x2-y2} and S/P p orbitals, as would be expected for the d^8 metal ion in a square planar field (Figure S90). The shift to higher energy for this transition as function of metal ion is consistent with the stronger ligand environment for the heavier metals and therefore higher energy for this σ^* MO. The calculated spectrum for [(pdt)Ni(dppb)] suggests that the higher energy shoulder at ~400 nm
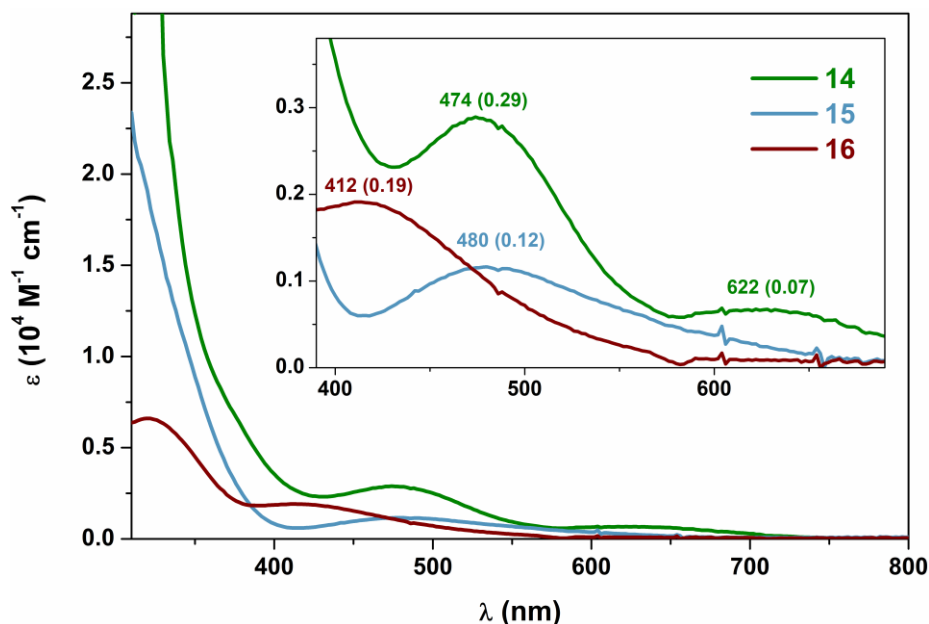
Figure 8. Overlay electronic absorption spectra (CH$_2$Cl$_2$) for **14**, **15**, and **16**.

for **4** and **5** is predominantly a pair of closely spaced dithiolene → dppb ligand-to-ligand charge transfer (LLCT) transitions (HOMO → LUMO+1, +2; *cf*. Table S12, Figure S90).

Time-dependent DFT calculations undertaken on [(pdt)Ni(μ-tpbz)Ni(pdt)] (Table S13) suggest that the probable assignment of its two lowest energy absorptions is the qualitatively the reverse of that indicated for [(adt)Ni(dppb)] because the π* MOs of the tpbz ligand are somewhat lower in energy than those of dppb. Thus, the lowest energy excitation in [(pdt)Ni(μ-tpbz)Ni(pdt)], **14**, is a superposition of closely spaced HOMO → LUMO, HOMO-1 → LUMO+1 transitions, which are essentially similar dithiolene → tpbz LLCT. The MOs involved have the same qualitative appearance as seen for their counterparts in **19** (Figure S88). These transitions are associated with the absorption at 622 nm in **14** and with higher energy bands in **15** and **16** (Figure 8) that contribute to the unresolved long tailing edge in their spectra. The next absorption bands calculated to be of significance in **14**, at 515 and 508 nm, are closely spaced HOMO and HOMO-1 transitions to the LUMO+2, which is a metal d$_{x2-y2}$ and Sp-Pp σ* combination. These excitations likely correspond to the maxima at 480 and 412 in **15** and **16**, respectively.

The nature of the redox processes in these dimetallic compounds was examined by spectroelectrochemical UV-vis methods, with compound **17** being selected as a representative subject for study. As noted, **17** exhibits two reversible oxidations (-0.04 V and +0.49 V) and a quasi-reversible reduction at -2.05 V vs Fc$^+$/Fc. Controlled potential bulk electrolysis at +0.2 V
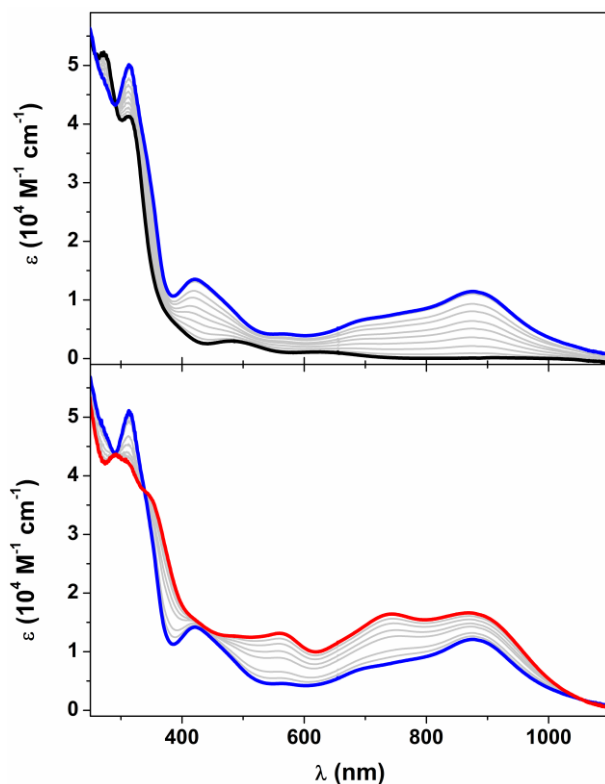
Figure 9. Changes in the electronic spectra during controlled potential electrolysis of **17** in CH_2Cl_2 solution (containing 0.1 M $[(^nBu)_4N][PF_6]$) at -25 °C. The first two-electron process is shown in the top panel where **17** (black) to oxidized to $[17]^{2+}$ (blue); changes attending the further two-electron oxidation of $[17]^{2+}$ (blue) to $[17]^{4+}$ (red) are shown in the bottom panel.

and concurrent monitoring of its electronic absorption profile revealed striking differences between **17** and *in situ* generated $[17]^{2+}$. Intense absorption by $[17]^{2+}$ in the near infrared region is assigned as intraligand charge transfer between reduced thiolate sulfur and sulfur radical (S^- →S˙) (Figure 9, top). Further oxidation of $[17]^{2+}$ to $[17]^{4+}$ at 0.8 V shows growth of different absorption maxima at ~550 nm and ~750 nm (Figure 9, bottom). These solution-generated oxidation products, $[17]^{2+}$ and $[17]^{4+}$, are well-behaved, although some bleaching was encountered with the $[17]^{4+}$ species. Controlled potential electrolysis of **17** at -2.1 V was examined, but the reduced species decomposed rapidly with no reversibility on the timescale of controlled potential coulometry.
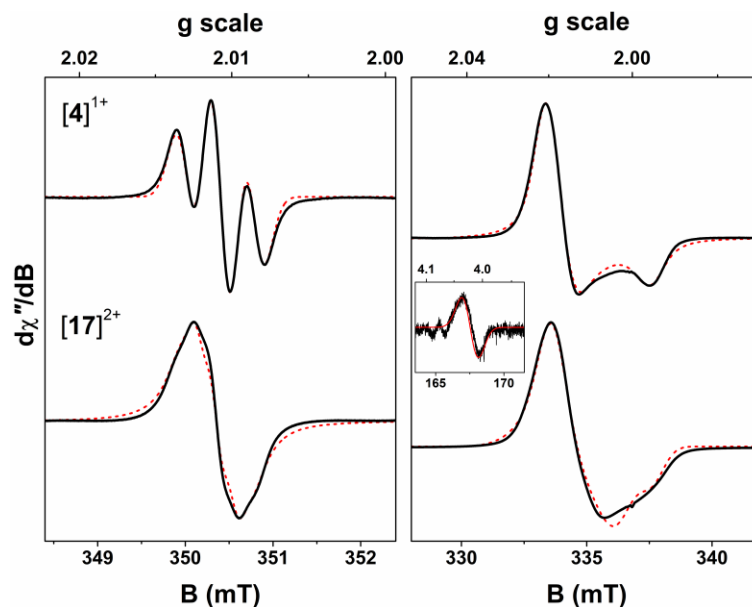
Figure 10. X-band EPR spectra of $[\mathbf{4}]^{1+}$ and $[\mathbf{17}]^{2+}$ recorded in CH_2Cl_2 solution at 293 K (left panel) and 130 K (right panel). Experimental data are shown by the black line and simulations depicted by the dashed red trace (conditions: frequency, 9.436 GHz; power, 0.63 mW; modulation, 0.1 mT). Inset on the right panel shows half-field signal with the simulation overlaid by the red line (conditions: frequency, 9.4291 GHz; power, 200 mW; modulation, 0.7 mT).

EPR Spectroscopy

The locus of the redox chemistry in this series is further probed by EPR spectroscopy. The *in situ* oxidation of **4** in dichloromethane produced an EPR spectrum consistent with a coordinated dithiolene radical bound to a Ni^{II} d^8 central ion. The fluid solution X-band spectrum of $[\mathbf{4}]^{1+}$ possess a binomial triplet splitting pattern from coupling of the electron spin to two equivalent ^{31}P ($I = \frac{1}{2}$, 100% abundant) nuclei of the dppb ligand (Figure 10). Simulation yielded spin-Hamiltonian parameters $g_{iso} = 2.0114$ and $A_{iso} = 3.5 \times 10^{-4}$ cm^{-1},[47] and closely matches spectra recorded for analogous compounds.[48] It is noteworthy that the hyperfine coupling in $[\mathbf{4}]^{1+}$ is larger than in the corresponding Pd compound $[\mathbf{5}]^{1+}$,[15] which arises from the greater contribution of Ni 3d and therein P 3p content in the SOMO due to the increased tetrahedralization of the NiP_2S_2 square plane compared with its heavier group 10 congeners (vide supra). Upon cooling to 130 K, the anisotropic spectrum is axial with $g = (2.0205, 2.0158, 1.9954)$ commensurate with an unpaired electron localized to the dithiolene ligand. The linewidth is sufficiently large to obscure any hyperfine splitting; nonetheless, the simulation was

improved by its inclusion ($A = (3.0, 3.5, 3.5) \times 10^{-4}$ cm^{-1}) to match its appearance at room temperature. This spectrum is identical to that recorded for [(pdt)Ni(dppe)]$^{1+}$ reported by Bowmaker *et al*. where dppe is 1,2-bis(diphenylphosphino)ethane.[48]

The fluid solution X-band EPR spectrum of [**17**]$^{2+}$ shows an isotropic line with less pronounced yet clearly visible ^{31}P hyperfine splitting (Figure 10). The spectrum was modelled with $g_{iso} = 2.0110$ and $A_{iso} = 1.75 \times 10^{-4}$ cm^{-1} on the basis of $S = 1$ coupling to four equivalent ^{31}P nuclei.[47] Most importantly, the ^{31}P hyperfine interaction is exactly half that in [**4**]$^{1+}$ indicative of a miniscule singlet-triplet gap (represented by the exchange coupling parameter, J'), though it is still larger than the Zeeman interaction ($h\nu = 0.3$ cm^{-1} at X-band).[49] A similar spectrum was previously reported for [**18**]$^{2+}$,[15] where again the ^{31}P superhyperfine coupling constant is smaller for this Pd analogue on account of its rigidly square planar geometry. The frozen solution spectrum of [**17**]$^{2+}$ recorded at 130 K is noticeably different to that of the spin-doublet spectrum of [**4**]$^{1+}$ (Figure 10). This spectrum is generated by superposition of two mono-spin signals where the broadening and linewidth variations are caused by the weak dipolar coupling – through space interaction – of the two unpaired electrons localized to either end of the complex. Following the analysis applied to [**18**]$^{2+}$,[15] the spectrum was successfully simulated utilizing an *effective* spin Hamiltonian for a spin-triplet state, where D and E/D parameterize the zero-field splitting of the triplet that arise from the spin-spin dipolar coupling (Eq. 5).

$$\hat{H} = D[\hat{S}_z^2 - \tfrac{1}{3}S(S+1) + E/D(\hat{S}_x^2 + \hat{S}_y^2)] + \mu_B \cdot \mathbf{B} \cdot g \cdot \mathbf{S} \qquad (5)$$

In this approach, singlet-triplet transitions are completely neglected, which is justified as $J' \gg h\nu$ and ^{31}P hyperfine interactions are absent in the experimental spectrum. An excellent fit was afforded with minute anisotropy, $g = (2.010, 2.017, 2.007)$ and a vanishingly small zero-field splitting, $D = -18 \times 10^{-4}$ cm^{-1} with negligible rhombicity, $E/D = 0.005$ (Figure 10). A ^{31}P hyperfine interaction of $A = (3, 1, 1) \times 10^{-4}$ cm^{-1} was included in the fit. The D-value is 20% larger than that determined for [**18**]$^{2+}$ of -15×10^{-4} cm^{-1},[15] matching the consistently larger ^{31}P hyperfine coupling for Ni complexes compared with the Pd analogues. Furthermore, a very weak forbidden "$\Delta M_s = 2$" transition between $|T, +1\rangle$ and $|T, -1\rangle$ triplet levels is revealed at $g = 4.019$ whose intensity is proportional to the magnitude of D (inset, Figure 10).

Since D owes its origin to the dipole interaction between the two dithiolene radicals, its value is a measure of the mean separation (r) of the two spin density distributions given by $D = -\tfrac{3}{2}g^2\mu_B^2 r^{-3}$ for $E/D = 0$ (where $\mu_B^2 = 0.433$ for D in cm^{-1} and r in Å).[49] The value for D of $-18 \times$

10^{-4} cm^{-1} for g_x = 2.010 obtained by simulation yields a corresponding distance of 11.3 Å between the two radicals, where the x-axis bisects the dithiolene and tpbz ligands.[50] The interspin distance is shorter than for [**18**]$^{2+}$ (r = 12.0 Å) because more unpaired spin is distributed to the Ni ions which reduces the separation between each barycenter in this spin-triplet. In addition, the interpsin distance is modulated by the distortion of the dimetallic complex which can bend and fold about the bridging tpbz ligand (Figure 4). Such a phenomenon is occurring here as it leads to a distribution of the interspin distances that leads to the significant line broadening that obscures most of the fine structure in the spectrum of [**17**]$^{2+}$ when compared with the prominent fine structure in [**18**]$^{2+}$.[15]

Summary and Concluding Remarks

In this report, we have detailed the synthesis and physical characterization of a set of dimetallic group 10 compounds in which redox-active dithiolene ligands are separated at a well-defined distance by 1,2,4,5-tetrakis(diphenylphosphino) benzene, which has an insulating quality to it. These compounds (**10–19**) are accessible on a preparative scale by several distinctly different routes. Such related monometallic compounds as assist the interpretation of the properties of their dimetallic homologues have also been prepared. Compounds **11–19** support very reversible oxidation to dications which possess a degenerate singlet diradical triplet ground state.

The collective observations in this work bring a degree of clarity to the attributes of this system that may be manipulated, and with what effect, upon the stability of the separated spins and the potential at which they are generated. Use of aryl-substituted dithiolene ligands (R = Ph, p-anisyl) confers greater chemical stability to the system upon oxidation than does R = Me, as judged by greater reversibility in the cyclic voltammetry. This greater stability vis-à-vis Me is attributed to moderate protection of the MS$_2$C$_2$ chelate π system by a ~30° canting of the aryl substituent with respect to the dithiolene chelate ring, which projects at least a modest steric profile both below and above the chelate ring. The electron donating nature of the p-anisyl group relative to the parent phenyl group manifests itself in oxidation potentials that are ~90 mV less oxidizing for the first oxidation of **11–19** and ~220 mV less so for the second. Thus, use of an aryl substituent with still more electron donating character (e.g., Me$_2$N-p-C$_6$H$_4$) may shift oxidation potentials to still milder potentials. Use of the (mnt)$^{2-}$ ligand removes accessible ligand

oxidation altogether and instead enables near simultaneous metal-based reductions, albeit with greater coupling because of the smaller separation. This smaller separation could be offset, however, by deliberate oxidation of the tpbz ligand to its phosphine oxide and coordination to M^{II} through oxygen rather than phosphorus.

The collected synthetic and structural work offered here emphasizes how very tractable these tpbz-linked molecules are toward scaled preparation, and handling in air, purification by chromatography and crystallization. These chemical characteristics may ultimately be essential to any practical application stemming from them. A considerable advantage to this general system is that the localization of spin on the organic dithiolene ligand brings the power and versatility of synthetic chemistry to bear for tailored effect. Furthermore, the localization of the spins to the S_2C_2 dithiolene chelate allows for a long coherence lifetime because these low Z elements do not have abundant natural isotopes with nuclear spin (^{13}C, $I = {}^1/_2$, 1.1% abundance; ^{33}S, $I = {}^3/_2$, 0.7% abundance). Minimization of contact of the electron spins with spin-active nuclei is crucial in generating long coherence lifetimes needed in quantum computing hardware.[51] In continuing work, we are examining the performance characteristics of these one- and two-qubit prototypes using pulsed EPR methods.

As a related vein of effort, we pursue the synthesis of elaborated, multi-metallic redox active molecules devised from open-ended molecules of the sort $[(S_2C_2R_2)M(\eta^2\text{-tpbz})]$, which are readily prepared and purified in scalable fashion. Closed polygonal molecules whose vertices are redox-active metallodithiolene fragments separated from one another at well-defined distance are also being targeted. Judicious "modular" implementation of tpbz, metal ion, and dithiolene ligand allows for highly controlled synthesis such that variable molecule size and variable number and spatial disposition of spins can be systematically explored. Because the building components can be changed deliberately, the all-important spin coupling can be controlled by synthetic chemistry. These proposed compounds offer new, previously unconsidered possibilities for applications in molecular-based spintronic devices and quantum hardware that will be the subject of future reports.

Associated Content

Supporting Information. Full description of procedures for crystal growth, diffraction data collection and processing, and structure solution and refinement; Complete crystallographic data

for all new structures in CIF format; Tables of crystal data and refinement statistics (Tables S1-S6); Thermal ellipsoid plots with complete atom labeling (Figures S1-S55); Electrochemistry for **1-2**, **4-6**, **10**-**19** (Figures S59-S87); Description of computational methods and coordinates for geometry-optimized structures of **4-6**, **10**, **19** (Tables S7-S11); MO energy level diagrams for **4-6** (Figures S56-S58), **19** (Figure S88), and **10** (Figure S89); TD-DFT calculated electronic transitions for **6** and **14** (Tables S12, S13, Figure S90). This material is available free of charge via the Internet at http://pubs.acs.org.

Accession Codes. CCDC 1582165-1582170, 1582172-1582185, and 1582187 contain the supplementary crystallographic data for this paper. These data can be obtained free of charge via www.ccdc.cam.ac.uk/data_request/cif, or by emailing data_request@ccdc.cam.ac.uk, or by contacting The Cambridge Crystallographic Data Centre, 12 Union Road, Cambridge CB2 1EZ, UK; fax: +44 1223 336033.

Author Information

Corresponding Authors

*E-mail: donahue@tulane.edu, Stephen.Sproules@glasgow.ac.uk

Notes

The authors declare no competing financial interest.

References

(**1**) Lim, B. S.; Fomitchev, D. V.; Holm, R. H. Nickel Dithiolenes Revisited: Structures and Electron Distribution from Density Functional Theory for the Three-Member Electron-Transfer Series [Ni(S$_2$C$_2$Me$_2$)$_2$]$^{0,1-,2-}$. *Inorg. Chem.* **2001**, *40*, 4257-4262.

(**2**) Bigoli, F.; Chen, C.-T.; Wu, W.-C.; Deplano, P.; Mercuri, M. L.; Pellinghelli, M. A.; Pilia, L.; Pintus, G.; Serpe, A.; Trogu, E. F. [Ni(R$_2$pipdt)$_2$](BF$_4$)$_2$ (R$_2$pipdt = 1,4-Disubstituted-piperazine-3,2-dithione) as Useful Precursors of Mixed-Ligand Dithiolenes of Interest for Non-linear Optics. *Chem. Commun.* **2001**, 2246-2247.

(**3**) Yan, Y.; Chandrasekaran, P.; Mague, J. T.; DeBeer, S.; Sproules, S.; Donahue, J. P. Redox-Controlled Interconversion between Trigonal Prismatic and Octahedral Geometries in a Monodithiolene Tetracarbonyl Complex. *Inorg. Chem.* **2012**, *51*, 346-361.

(**4**) Yu, R.; Arumugam, K.; Manepalli, A.; Tran, Y.; Schmehl, R.; Jacobsen, H.; Donahue, J. P. Reversible, Electrochemically Controlled Binding of Phosphine to Iron and Cobalt Bis(dithiolene) Complexes. *Inorg. Chem.* **2007**, *46*, 5131-5133.

(**5**) Wang, K.; Stiefel, E. I. Toward Separation and Purification of Olefins Using Dithiolene Complexes: An Electrochemical Approach. *Science* **2001**, *291*, 106-109.

(**6**) Dang, L.; Shibl, M. F.; Yang, X.; Alak, A.; Harrison, D. J.; Fekl, U.; Brothers, E. N.; Hall, M. B. The Mechanism of Alkene Addition to a Nickel Bis(dithiolene) Complex: The Role of the Reduced Metal Complex. *J. Am. Chem. Soc.* **2012**, *134*, 4481-4484.

(**7**) Dang, L.; Shibl, M. F.; Yang, X.; Harrison, D. J.; Alak, A.; Lough, A. J.; Fekl, U.; Brothers, E. N.; Hall, M. B. Apparent Anti-Woodward-Hoffman Addition to a Nickel Bis(dithiolene) Complex: The Reaction Mechanism Involves Reduced, Dimetallic Intermediates. *Inorg. Chem.* **2013**, *52*, 3711-3723.

(**8**) Baudron, S. A.; Hosseini, M. W. Modular Construction of a Series of Heteronuclear Metallamacrocycles. *Chem. Commun.* **2008**, 4558-4560.

(**9**) Velázquez, C. S.; Baumann, T. F.; Olmstead, M. M.; Hope, H.; Barrett, A. G. M.; Hoffman, B. M. Star Porphyrazines: Peripheral Chelation of Porphyrazineoctathiolate by Diphosphinonickel Ions. *J. Am. Chem. Soc.* **1993**, *115*, 9997-10003.

(**10**) Gan, L.; Groy, T. L.; Tarakeshwar, P.; Mazinani, S. K. S.; Shearer, J.; Mujica, V.; Jones, A. K. A Nickel Phosphine Complexas a Fast and efficient Hydrogen Production Catalyst. *J. Am. Chem. Soc.* **2015**, *137*, 1109-1115.

(**11**) Maisela, L. L.; Crouch, A. M.; Darkwa, J.; Guzei, I. A. Bidentate Aryldichalcogenide Complexes of [(Diphosphino)ferrocene]palladium(II) and [(Diphosphino)ferrocene]platinum(II). Synthesis, Molecular Structures and Electrochemistry. *Polyhedron* **2001**, *20*, 3189-3200.

(**12**) Qin, Y.-H.; Wu, M.-M.; Chen, Z.-N. Synthesis and Crystal Structure of a Heterotrinuclear Compound [PdCu$_2$(tdt)(μ-dppm)$_2$(MeCN)$_4$](ClO$_4$)$_2$·^{2}/$_3$H$_2$O (tdt = 3,4-toluenedithiolate, dppm = 1,2-bis(diphenylphosphino)methane). *Chin. J. Struct. Chem.* **2005**, *24*, 621-624.

(**13**) Arumugam, K.; Yu, R.; Villgrán, D.; Gray, T. G.; Mague, J. T.; Donahue, J. P. A Convergent Approach to the Synthesis of Multimetallic Dithiolene Complexes. *Inorg. Chem.* **2008**, *47*, 5570-5572.

(**14**) Arumugam, K.; Shaw, M. C.; Chandrasekaran, P.; Villagrán, D.; Gray, T. G.; Mague, J. T.; Donahue, J. P. Synthesis, Structures and Properties of 1,2,4,5-Benzenetetrathiolate Linked Group 10 Metal Complexes. *Inorg. Chem.* **2009**, *48*, 10591-10607.

(**15**) Arumugam, K.; Shaw, M. C.; Mague, J. T.; Bill, E.; Sproules, S.; Donahue, J. P. Long Range Spin Coupling: A Tetraphosphine-Bridged Palladium Dithiolene Dimer. *Inorg. Chem.* **2011**, *50*, 2995-3002.

(**16**) McFarlane, H. C. E.; Mcfarlane, W. A Convenient One-Pot Synthesis of *o*-Phenylene Bis(diphenylphosphine). *Polyhedron* **1983**, *2*, 303-304.

(**17**) McFarlane, H. C. E.; McFarlane, W. Polyphosphorus Ligands – V.* The Synthesis, Phosphorus-31 NMR Spectra and Conformations of the Polykis(diphenylphosphine) Benzenes $(Ph_2P)_nC_6H_{6-n}$ (n = 1-4). *Polyhedron* **1988**, *7*, 1875-1879.

(**18**) Davison, A.; Holm, R. H. Metal Complexes Derived from *cis*-1,2-Dicyano-1,2-ethylenedithiolate and Bis(trifluoromethyl)-1,2-dithiete. *Inorg. Synth.* **1967**, *10*, 8-25.

(**19**) Chandrasekaran, P.; Donahue, J. P. Synthesis of 4,5-Dimethyl-1,3-dithiol-2-one. *Org. Synth.* **2009**, *86*, 333-343.

(**20**) Chandrasekaran, P.; Greene, A. F.; Lillich, K.; Capone, S.; Mague, J. T.; DeBeer, S.; Donahue, J. P. A Structural and Spectroscopic Investigation of Octahedral Platinum Bis(dithiolene) Phosphine Complexes: Phosphine Association Induced by Platinum-Dithiolene Internal Redox Chemistry. *Inorg. Chem.* **2014**, *53*, 9192-9205.

(**21**) Ma, C.; Han, Y.; Li, D. Synthesis and Crystal Structures of Diorganotin Dicyanoethylene-1,2-Dithiolate Compounds and Their Derivatives with 4,4′-Bipy or Phen. *Polyhedron* **2004**, *23*, 1207-1216.

(**22**) Chandrasekaran, P.; Arumugam, K.; Jayarathne, U.; Pérez, L. M.; Mague, J. T.; Donahue, J. P. Synthesis, Structures, and Properties of Mixed Dithiolene-Carbonyl and Dithiolene-Phosphine Complexes of Tungsten. *Inorg. Chem.* **2009**, *48*, 2103-2113.

(**23**) Levason, W.; McAuliffe, C. A. Bidentate Ligands Containin Very Soft Donor Atoms: Nickel(II) Complexes of Aryarsines and Arylstibines. *Inorg. Chim. Acta* **1974**, *11*, 33-40.

(**24**) McFarlane, H. C. E.; McFarlane, W. Synthesis and NMR Spectra of Derivatives of the *polykis*(diphenylphosphino)benzenes, $(Ph_2P)_nC_6H_{6-n}$ [n = 2 to 4]. *Polyhedron* **1999**, *18*, 2117-2127.

(**25**) Boudier, A.; Breuil, P.-A. R.; Magna, L.; Olivier-Bourbigou, H.; Braunstein, P. Nickel(II) Complexes with Imino-imidazole Chelating Ligands Bearing Pendant Donor Groups (SR, OR, NR_2, PR_2) as Precatalysts in Ethylene Oligomerization. *J. Organonmet. Chem.* **2012**, *718*, 31-37.

(**26**) Menozzi, E.; Busi, M.; Ramingo, R.; Campagnolo, M.; Geremia, S.; Dalcanale, E. Design and Self-Assembly of Ditopic and Tetratopic Cavitand Complexes. *Chem. Eur. J.* **2005**, *11*, 3136-3148.

(**27**) Schrauzer, G. N.; Mayweg, V. P. Preparation, Reactions, and Structure of Bisdithio-α-diketone Complexes of Nickel, Palladium, and Platinum. *J. Am. Chem. Soc.* **1965**, *87*, 1483-1489.

(**28**) Drew, D.; Doyle, J. R. Cyclic Diolefin Complexes of Platinum and Palladium. *Inorg. Synth.* **1990**, *28*, 346-349.

(**29**) Armarego, W. L. F.; Perrin, D. D. *Purification of Laboratory Chemicals*, 4th ed.; Butterworth-Heinemannn: Oxford, U.K., 2000.

(**30**) Hanson, G. R.; Gates, K. E.; Noble, C. J.; Griffin, M.; Mitchell, A.; Benson, S. XSophe-Sophe-XeprView®. A computer simulation software suite (v. 1.1.3) for the analysis of continuous wave EPR spectra. *J. Inorg. Biochem.* **2004**, *98*, 903-916.

(**31**) Davison, A.; Edelstein, N.; Holm, R. H.; Maki, A. H. Further Examples of Compounds Related by Electron-Transfer Reactions: Complexes Derived from Bis(trifluoromethyl)-1,2-Dithiete. *Inorg. Chem.* **1964**, *3*, 814-823.

(**32**) Mayweg, V. P.; Schrauzer, G. N. Bis-adducts of Group VIII Metal Bisdithiobenzil Complexes with Phosphines. *Chem. Commun.* **1966**, 640-641.

(**33**) Usón, R.; Vicente, J.; Oro, J. Maleonitriledithiolate Complexes of Au(III), Au(I), Pd(II), and Pt(II) Containing Neutral or Anionic Ligands. *Inorg. Chim. Acta* **1981**, *52*, 29-34.

(**34**) Cerrada, E.; Fernández, E. J.; Concepción Gimeno, M.; Laguna, A.; Laguna, M.; Terroba, R.; Dolores Villacampa, M. Synthesis of Dithiolate Gold(III) Complexes by Dithiolate Transfer Reactions. X-ray Structure of [Au(C$_6$F$_5$)(S$_2$C$_6$H$_4$)(PPh$_3$)]. *J. Organomet. Chem.* **1995**, *492*, 105-110.

(**35**) Cerrada, E.; Fernández, E. J.; Jones, P. G.; Laguna, A.; Laguna, M.; Terroba, R. Synthesis and Reactivity of Trinuclear Gold(III) Dithiolate Complexes. X-Ray Structure of [Au(C$_6$F$_5$)(S$_2$C$_6$H$_4$)]$_3$ and [Au(C$_6$F$_5$)(S$_2$C$_6$H$_4$)I(SC$_6$H$_4$SPPh$_3$)]. *Organometallics* **1995**, *14*, 5537-5543.

(**36**) Nomura, M.; Fourmigué, M. Dinuclear Cp* Cobalt Complexes of the 1,2,4,5-Benzenetetrathiolate Bischelating Ligand. *Inorg. Chem.* **2008**, *47*, 1301-1312.

(**37**) Bevilacqua, J. M.; Zuleta, J. A.; Eisenberg, R. Luminescent Diphosphine Dithiolate Complexes of Platinum(II): Synthesis, Characterization, and Structure. *Inorg. Chem.* **1994**, *33*, 258-266.

(**38**) Huheey, J. E. *Inorganic Chemistry: Principles of Structure and Reactivity*, 3rd ed.; Harper & Row: New York, 1983; Chapter 9.

(**39**) Landis, K. G.; Hunter, A. D.; Wagner, T. R.; Curtin, L. S.; Filler, F. L.; Jansen-Varnum, S. A. The Synthesis and Characterization of Ni, Pd, and Pt Maleonitriledithiolate Complexes: X-ray Crystal Structures of the Isomorphous Ni, Pd, and Pt (Ph$_2$PCH$_2$CH$_2$PPh$_2$)M(maleonitriledithiolate) Congeners. *Inorg. Chim. Acta* **1998**, *282*, 155-162.

(**40**) Wrixon, J. D.; Hayward, J. J.; Raza, O.; Rawson, J. M. Oxidative Addition Chemistry of Tetrathiocines: Synthesis, Structures and Properties of Group 10 Dithiolate Complexes. *Dalton Trans.* **2014**, *43*, 2134-2139.

(**41**) Minenkov, Y.; Singstad, Å.; Occhipinti, G.; Jensen, V. R. The accuracy of DFT-optimized geometries of functional transition metal compounds: a validation study of catalysts for olefin metathesis and other reactions in the homogeneous phase. *Dalton Trans.* **2012**, *41*, 5526-5542.

(**42**) Shin, K.-S.; Son, K.-I.; Kim, K. I.; Hong, C. S.; Suh, M.; Noh, D.-Y. Heteroleptic Binuclear Palladium(II) and Platinum(II) Complexes Containing 1,2-Bis(diphenylphosphino)acetylene and 1,2-Benzenedithiolates: Syntheses, Crystal Structures, Electrochemistry and Photoluminescence Properties. *Dalton Trans.* **2009**, 1767-1775.

(**43**) Shin, K.-S.; Noh, D.-Y. Binuclear Paltinum(II) Building-Blocks for the Metal-Coordinated Self-Assembly: (Dithiolate)Pt(μ-dppa)₂Pt(dithiolate) where dppa = Bis(diphenylphosphino)acetylene. *Bull Korean Chem. Soc.* **2004**, *25*, 130-132.

(**44**) Wang, P.-W.; Fox, M. A. Metal-Metal Interactions in Tetrakis(diphenylphosphino)benzene-Bridged Dimetallic Complexes and Their Related Coordination Polymers. *Inorg. Chem.* **1994**, *33*, 2938-2945.

(**45**) Bowmaker, G. A.; Williams, J. P. Electrochemical, Electron Spin Resonance and Nuclear Magnetic Resonance Investigations of Tertiary Phosphine Complexes of Nickel. Part 1. Mono- and Di-Nuclear Nickel Dithiolene and Nickel Dihalide Species. *J. Chem. Soc., Dalton Trans.* **1993**, 3593-3600.

(**46**) Richardson, D. E.; Taube, H. Determination of $E_2° − E_1°$ in Multistep Charge Transfer by Stationary-Electrode Pulse and Cyclic Voltammetry: Application to Binuclear Ruthenium Ammines. *Inorg. Chem.* **1981**, *20*, 1278-1285.

(**47**) Fluid solution spectra were simulated using $\hat{H} = g \cdot \mu_B \cdot B \cdot S + \Sigma a_j \cdot S \cdot I$, where $S = {}^1/_2$ for [**4**]$^{1+}$ and $S = 1$ for [**17**]$^{2+}$.

(**48**) Bowmaker, G. A.; Boyd, P. D. W.; Campbell, G. K. Electrochemical and ESR Studies of the Redox Reactions of Nickel(II), Palladium(II), and Platinum(II) Complexes of 1,2-Diphenyl-1,2-ethenedithiolate(2–)-*S*,*S'*. *Inorg. Chem.* **1983**, *22*, 1208-1213.

(**49**) (**a**) Eaton, S. S.; More, K. M.; Sawant, B. M.; Eaton, G. R. Use of the ESR Half-Field Transition to Determine the Interspin Distance and the Orientation of the Interspin Vector in Systems with Two Unpaired Electrons. *J. Am. Chem. Soc.* **1983**, *105*, 6560-6567. (**b**) Eaton, S. S.; Eaton, G. R. EPR Studies of Long-Range Intramolecular Electron-Electron Exchange Interaction. *Acc. Chem. Res.* **1988**, *21*, 107-113.

(**50**) Kirmse, R.; Stach, J.; Dietzsch, W.; Steimecke, G.; Hoyer, E. Single-crystal EPR Studies on Nickel(III), Palladium(III), and Platinum(III) Dithiolene Chelates Containing the Ligands Isotrithionedithiolate, *o*-Xylenedithiolate, and Maleonitriledithiolate. *Inorg. Chem.* **1980**, *19*, 2679-2685.

(**51**) Sproules, S. Molecules as Electron Spin Qubits. In *Electron Paramagnetic Resonance;* Chechik, V. and Murphy, D. M., Eds.; Royal Society of Chemistry: 2017; pp. 61-97.

For Table of Contents Use Only
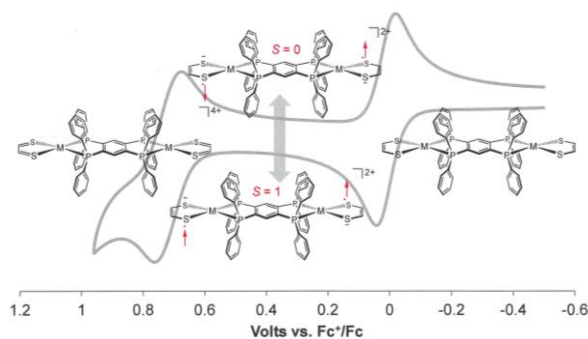
Synopsis. Compounds of the type $[(S_2C_2R_2)M(\mu\text{-tpbz})M(S_2C_2R_2)]$ (R = CN, Me, Ph, *p*-anisyl; M= Ni, Pd, Pt; tpbz = 1,2,4,5-tetrakis(diphenylphosphino)benzene) have been synthesized and reveal a range of topologies (undulating, chair, bowed) for the $(S_2C_2)M(P_2C_6P_2)M(S_2C_2)$ core. Electrochemically, the compounds support reversible oxidations (R = Me, Ph, *p*-anisyl) or reductions (R = CN) attributable to nearly concurrent processes at the identical ends of the molecule because of the tpbz ligand's electronically insulating character.